Surface modification of polysulfone (PSF) nanofiber by surface segregation

Fluorine enrichment of electrospun PSF nanofiber surface and superhydrophobicity

Use of small amount of fluorinated polyurethane active additive (FPA)

Improved mechanical properties of self-sustained FPA blended PSF nanofibrous membrane

Suitable characteristics for desalination by direct contact membrane distillation

Competitive and stable permeate fluxes without interfiber space wetting were achieved

PSF nanofiber

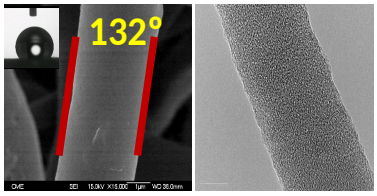

LEP_w (PSF) = 23.4 kPa

FPA
(4.5 wt%)

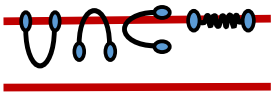

Aligned on Surface
or Combination

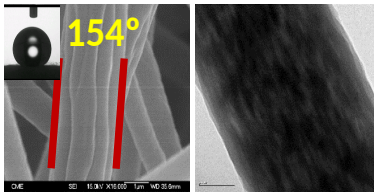

LEP_w (PSF/FPA) = 96.2 kPa ⬆

DCMD (T_f=80°C, T_p=20°C)

Wetting

> 99.996%!!

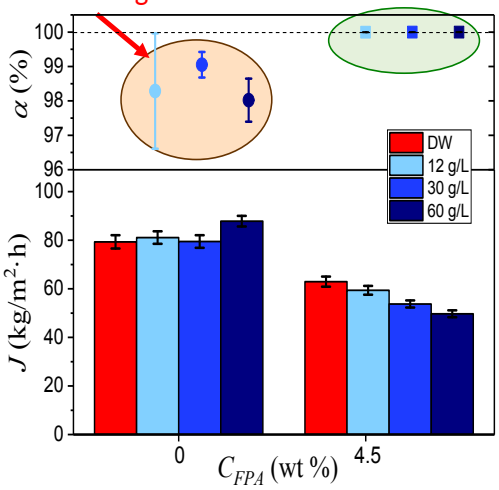

Superhydrophobic Nanofibers Electrospun by Surface Segregating Fluorinated Amphiphilic Additive for Membrane Distillation

M. Khayet[1,2,*], C. García-Payo[1], T. Matsuura[3]

[1] Department of Structure of Matter, Thermal Physics and Electronics, Faculty of Physics, University Complutense of Madrid, Avda. Complutense s/n 28040 Madrid (Spain)

[2] Madrid Institute of Advances Studies of Water (IMDEA Water Institute), Calle Punto Com n° 2, 28805 Alcalá de Henares, Madrid (Spain)

[3] Department of Chemical and Biological Engineering, University of Ottawa, 161 Louis Pasteur St., Ottawa, ON, K1N 6N5 (Canada)

* Corresponding authors: khayetm@ucm.es (M. Khayet)

Abstract

A facile route for the in situ surface modification and mechanical strength-enhancement of electrospun nanofibers is described. Blends of a host hydrophilic polymer, polysulfone (PSF), and small quantities of a fluorinated polyurethane additive (FPA) up to 6 wt% in the PSF blend were considered. During electrospinning, this additive undergoes spontaneous surface segregation resulting in nanofibers with an improved hydrophobic character attributed mainly to the detected fluorine-rich surface and enhanced mechanical properties. We report the effects of the fluorinated additive content in the blend on the morphological and structural characteristics of the electrospun nanofibrous mats (ENMs) including their inter-fiber space and void volume fraction. ENMs with a superhydrophobic surface could be prepared using at least 3 wt% FPA in the PSF blend. The ENMs were tested in desalination by membrane distillation (MD) and competitive permeate fluxes as high as 53.8 kg/m^{2}h, with stable low permeate electrical conductivities (< 5.1 μS/cm), were achieved for the ENM prepared with 4.5 wt% FPA in the PSF blend, when the feed was 30 g/L NaCl aqueous solution and the transmembrane temperature difference was 60°C, without any inter-fiber space wetting being detected.

Keywords: Nanofiber; surface modification; electrospinning; fluorinated polyurethane; polysulfone; superhydrophobicity; membrane distillation.

1. Introduction

By means of the application of a high-voltage electrostatic field, electrospinning has become a versatile and a broadly used technique in diverse research areas to produce ultra-thin fibers from homopolymers, copolymers and polymers blends with great interests in a range of applications such as medicine, sensor technology, optoelectronics, tissue engineering and filtration technology [1-5]. Surface-functionalized electrospun fibers have been proposed using different procedures such as coaxial electrospinning [6], surface coating [7,8], grafting [9], plasma treatment [10-12], physical or chemical vapor deposition [13-16]. Except the first method, the other approaches involve at least one post-spinning process and the use of hazardous restricted chemicals. Besides, post-processing introduces undesirable effects such as pore blockage, involves high risks to damage the nanofiber structure and results in uncontrollable amount and thickness of functional molecules on the nanofiber surface. A facile route for surface functionalization of electrospun nanofibers is through spontaneous surface segregation of fluorinated additives that are able to migrate to the surface of the fiber, changing its characteristics [17,18]. For such segregation, the active additive must have a lower surface free energy than that of the host polymer, which is generally a more hydrophilic polymer. Thus, if the additive sufficiently migrates to the nanofiber surface during electrospinning, the need for an extra step can be avoided. The lessons learned from previous research studies on thin film and hollow fiber surface migration of low surface energy active additives, can be applied to nanofibers prepared by electrospinning. It may be suggested that one of the important parameters affecting this migration is the necessary time for solvent evaporation between casting or spinning the polymer solution and the immersion in the coagulation bath for the formation of thin films and hollow fibers, respectively. For thin films this time can be controlled to the desired length, but for the preparation of hollow fibers and electrospun nanofibers

this time is limited and depends mainly on the gap distance between the spinneret or metallic needle to the coagulation bath or metallic collector. For hollow fibers, the effects of the air gap on the surface chemistry and morphology were studied for different hydrophilic host polymers such as polyetherimide (PEI) or polyethersulfone (PES) and surface active additives such as fluorinated surface modifying macromolecules (i.e. SMMs) [19,20]. The hydrophobic character of the outer surface of the hollow fibers was enhanced by the increase of the air gap distance, confirming SMMs migration without significantly affecting the physical properties of the host polymer as only small amounts of SMMs were normally added (i.e. < 5 wt% in the polymer solution). Besides, the SMMs modified materials exhibited higher chemical resistance and mechanical strength than the unmodified ones. So far, most of the studies have been focused on SMMs surface modification to make the flat sheet more hydrophobic [21-24]. As well, other fluorinated additives have also been investigated to render the surfaces not only hydrophobic but also superhydrophobic [25-28].

Various attempts have been made to produce surface modified electrospun nanofibers by adopting the surface segregation strategy in the presence of an electric field, which affects significantly the movement and distribution of ionic species in the formed nanofiber [17,29-36]. For instance, during electrospinning the negatively charged species can be preferentially driven by the positive polarity of the electric field source to the Taylor cone and electrospun jet surfaces, resulting in nanofibers with a tailored surface composition [29-31].

When using fluorinated compounds, because of their low surface free energy, it is generally accepted that the fluorinated segments or end groups tend to migrate towards the surface/air interface, changing their surface characteristics. Hunley *et al.* [33] prepared hydrophobic electrospun PMMA nanofibers by adding hyperbranched polyethylenimine partially functionalized with perfluorinated and aliphatic end-groups (PFA). It was observed that the

selective segregation of PFA to the nanofiber surface depended on its concentration in the polymer solution. Bianco *et al.* [34] detected an increase of the water contact angle from 61º for an unmodified polyamide (PA6) nanofibrous web to 123º for the polyamide nanofibers doped with 6% perfluorinated acridine. It was claimed that thermal annealing near the glass transition temperature (T_g) of the polymer improved the surface migration of the perfluorinated alkyl chains. Polystyrene electrospun superhydrophobic nanofibers with high surface fluorine segregation were prepared using a series of fluoroalkyl end-functionalized polystyrene additives [17]. Spontaneous surface migration of these additives during electrospinning resulted in fluorine-rich and superhydrophobic surfaces. Superhydrophobic surfaces of electrospun nanofibers were also fabricated using a perfluorinated linear diol (fluorolink-D), a copolymer of acrylonitrile and α,α-dimethyl-*meta*-isopropenylbenzyl isocyanate [35]. Wu *et al.* [36] successfully prepared superhydrophobic electrospun polyurethane elastomers containing perfluoropolyether segments (FPU) with different geometrical nano- and micro-structured surfaces. It was concluded that the micro- and nano-scale surface roughness enhanced the water contact angle to values above 150º but low surface energy surfaces alone due to fluorine migration could not provide a self-cleaning effect. Abnormal fluorine aggregation was detected by the same authors in FPU nanofibers prepared by electrospinning and the subsequent depletion of fluorine content on their surfaces [37]. This was explained by means of the dynamic light scattering and fluorescence analysis and by the higher concentration of FPU in the polymeric solutions than the aggregation transition concentration (i.e. formation of FPU chains aggregation). In poor solvents such as tetrahydrofuran (THF) and *N*,*N*-dimethyl formamide (DMF), perfluoropolyether segments of FPU were found to be wrapped inside the hydrogen segments. During electrospinning, the rapid solvent evaporation

and fast formation of nanofibers occurred so that there was not enough time for the perfluoropolyether segments to be unwrapped and segregated to the surface.

Based on the above cited studies, it could be stated that a maximum surface enrichment of electrospun nanofibers would be accomplished when the polymer contains opposite polarity groups in the side chain. An amphiphilic graft copolymer, poly(methyl methacrylate-ran-hydroxypropyl acrylate)-graft-poly(dodecafluoroheptyl methacrylate) (PMMA-r-PHPA-g-PDFMA), with hydrophobic PDFMA segments and amphiphilic hydroxyl groups in the side chain was used to prepare superhydrophobic electrospun nanofibers [38]. Highly fluorinated surfaces associated to the PDFMA segments were obtained with small amounts of the fluoromonomer. This was also attributed to the opposite bulk segregation of –OH group as the spinneret was connected to the positive electrode. Perfluorinated poly(2,2,2-trifluoroethyl methacrylate) (PTFEMA) homopolymer was synthesized and used for the preparation of electrospun nanofibers with superamphiphobicity that was attributed to the surface enrichment of fluorine (i.e. water and hexane contact angles exceeded 150^{o}) [39]. It is worth quoting that only few studies have been focused on the use of low amounts of fluorinated active additives in the dope solution (i.e. below 10 wt %) for the preparation of electrospun fluorinated and superhydrophobic nanofibers [17,33, 34].

In general, for the preparation of superhydrophobic electrospun nanofibrous mats (ENMs), fluoropolymers are preferred to other materials because of their extremely low surface free energy and excellent properties such as the high resistances to acid and alkali due to the presence of electronegative fluorine atoms. In the present study, blends of a host hydrophilic polymer, polysulfone (PSF), and small quantities of a fluorinated polyurethane additive (FPA), up to 6 wt %, in PSF blend have been considered to prepare novel superhydrophobic surface modified

electrospun nanofibers in one step. FPA enrichment at the surface of the nanofibers was observed resulting in superhydrophobic ENMs with only 3 wt % FPA in the PSF blend together with improved mechanical properties. These ENMs exhibited desirable characteristics for desalination by membrane distillation (MD). PSF polymer is an attractive membrane material having excellent chemical resistance and good thermal stability but its hydrophobic character is too weak to be suitable for MD separation (i.e. water contact angle, θ = 82.3 ± 2.1º) [40-42]. It is also worth mentioning that very few studies have been focused on the design of superhydrophobic MD membranes although these types of membranes proved to be more stable in MD performance than others [40-42].

2. Experimental

2.1. Materials

Polysulfone (PSF, UDEL P-3500 LCD, Solvay Specialty Polymers; M_w = 79,000 g/mol; ρ = 1.24 g/mL) was used as the host polymer to prepare the surface modified nanofiber. PSF was first dried at 120 °C in a vacuum desiccator placed in a heating mantle (Selecta) and connected to a vacuum pump (Vacuubrand brand, model MZ2C). Acetone and *N*,*N*-dimethyl acetamide (DMAC) purchased from Sigma-Aldrich were used to prepare the electrospinning solutions. POREFIL® (Porometer) and isopropyl alcohol (IPA, Sigma-Aldrich) were used as wetting liquids for the measurements of the inter-fiber space (d_i) and the void volume fraction (ε), respectively. Sodium chloride (NaCl, Panreac) was used to prepare the salt aqueous feed solutions for the measurements of the liquid entry pressure (*LEP*) and the direct contact membrane distillation (DCMD) tests. For the synthesis of the fluorinated polyurethane additive (FPA), other than DMAC and acetone, the

following materials were employed: 4,4′-Methylene bis(phenyl isocyanate) (MDI, 98%, Sigma Aldrich) for the di-isocyanate, 4,4´-sulfonyldiphenyl (Dihydroxy diphenyl sulfone, DPS, 98%, Sigma-Aldrich) for the diol and Zonyl fluorotelomer intermediate 2-(perfluoroalkyl) ethanol (FAE, BA-L, M_w = 443 Da and 70 wt % fluorine, DuPont product supplied by Aldrich Chemical Co., Inc., 98%) for the oligomeric fluoro-alcohol.

2.3. Synthesis and characterization of FPA

The fluorinated polyurethane additive (FPA) was synthesized in a controlled nitrogen (N_2) gas atmosphere following the two-step solution polymerization method illustrated in **Figure S1** and detailed elsewhere [43]. The solvent DMAC was first distilled at 25°C under a pressure of 133.3 Pa, whereas MDI was distilled at 150ºC under a pressure of 66.7 Pa. The polyol DPS as well as the fluoro-alcohol (FAE) were degassed for 24 h under a pressure of 66.7 Pa. In the first polymerization step the MDI was reacted with the DPS in the solvent DMAC to form the pre-polymer polyurethane (PU). This is subsequently end-capped by the addition of FAE in the second polymerization step to obtain the FPA. The stoichiometric molar ratio of MDI/DPS/FAE was 3/2/2. The formed FPA was precipitated from the solution (FPA in DMAC) with distilled water under mechanical stirring to remove any residual solvent, washed at least three times in 30% acetone/water mixture (i.e. 30/70 by volume) to leach out the unreacted monomer and finally dried first in an oven with forced air circulation at 50ºC for 48 h and then under vacuum at 35ºC for additional 48 h. The chemical structure and characteristics of the synthesized FPA are also shown in **Figure S1**. The fluorine content (F) and the polystyrene equivalent molecular weights (i.e. the weight average molecular weight, M_w, and the number average molecular weight, M_n) of the FPA

additive were determined following the methodology and using the instrument detailed elsewhere [23,24,43]. In the present study, the synthesized FPA exhibited a high fluorine content (20.0 wt %) and low molecular weights (**Figure S1**).

2.4. Preparation of modified PSF nanofibers

First, 25 wt % PSF was dissolved in 80/20 wt % DMAC/acetone mixture at 50ºC in an orbital shaker thermostatic bath (Stuart SBS40) during 24 h and then subjected to magnetic stirring agitation of 120 rpm for about 4 h until the complete dissolution of the polymer, followed by the addition of the different amounts of FPA (0 - 6 wt %). **Table 1** shows the FPA concentration in the blend (FPA/PSF) solution and the concentration based on the PES weight. The table also summarizes the measured surface tension (γ_p), electrical conductivity (σ_p) and viscosity (μ_p) at 23 ± 1ºC of the blend (FPA/PSF) solutions. The surface tension was measured using the pendant drop shape acquired by an optical contact angle meter (CAM200), the electrical conductivity was measured by the conductivity meter (Cyber Scan con11 Conductivity/TDS/1C, Eutech Instruments) and the viscosity by a Digital Viscometer (Brookfield, DV-I+) connected to a thermostat (Model HETO21-DT-1, Rego S.A). Details of these measurements can be found elsewhere [44]. Prior to characterization and electrospinning of nanofibers, the polymer blends were left to degas overnight at room temperature.

Electrospinning was carried out using a laboratory made system described in our previous study [45]. A glass syringe (Nikepal, 20 mL) clamped to a circulation pump (KDS-200, Scientific) and connected to a metallic needle (0.6/0.9 mm inner/outer diameters) was first filled with the polymer blend, which was extruded through the needle with a flow rate of 1.1 mL/h. A positive DC voltage

of 20 kV was applied near the tip of the needle in order to form a stable electrified jet flow by a high voltage digital power supply (Iseg; model T1CP 300 304P; 1x30 kV/0.3 mA) with an adjustable voltage in the range 0 - 30 kV. The electric current was below 2 μA. The nanofibers were assembled on a grounded metallic collector placed 25 cm from the needle tip. The ambient temperature and relative humidity were 23 ± 1 °C and 37.5 ± 2%, respectively. The obtained electrospun nanofibrous mats (ENMs) during 1 h electrospinning time were dried in a vacuum oven at 120 °C for 2 h to remove any residual solvent(s). The resultant ENMs from 0, 1.5, 3, 4.5 and 6 wt % FPA blended in the PSF solution (i.e. 0, 6, 12, 18 and 24 % based on PSF polymer weight) were denoted hereafter as PSF-0, PSF-1.5, PSF-3, PSF-4.5, PSF-6, respectively.

Table 1. *Surface tension (γ_p), electrical conductivity (σ_p), viscosity (μ_p) of the PSF and FPA blended PSF solutions as well as nanofiber diameter (d_f) of the prepared ENMs.*

ENMs	C_{FPA} (wt %)	C_{FPA} (%) [a]	γ_p (mN/m)	σ_p (μS/cm) [b]	μ_p (Pa.s)	d_f (nm)
PSF-0	0	0	41.8 ± 0.5	2.17 ± 0.01	2.00 ± 0.01	78 ± 15
PSF-1.5	1.5	6	27.0 ± 1.8	2.27 ± 0.01	3.28 ± 0.11	91 ± 18
PSF-3	3	12	25.6 ± 0.4	2.57 ± 0.04	4.83 ± 0.05	126 ± 26
PSF-4.5	4.5	18	25.0 ± 0.4	2.72 ± 0.02	6.15 ± 0.05	440 ± 130
PSF-6	6	24	23.3 ± 0.4	2.86 ± 0.01	7.35 ± 0.06	561 ± 80

[a] Amounts based on the PSF polymer weight

[b] σ_p = 0.50 ± 0.01 μS/cm of 80/20 wt % DMAC/acetone mixture

2.5. Characterization of modified nanofibers and ENMs

The surface and cross-section of the nanofiber were examined by the field emission scanning electron microscope (FE-SEM, JEOL Model JSM-6335F) equipped with the X-ray energy dispersive spectrometer (EDX, Oxford Instruments). The cross-sections of the samples were prepared by fracturing the ENMs in liquid nitrogen. All samples were gold coated by a rotary-pumped sputter coater (QUORUM Q150R S) for 60 s at 20 mA. Both the surface and the cross-section were analyzed by EDX using the software INCA (Oxford Instruments) to determine the elemental composition of carbon, oxygen, fluorine, sulfur, and nitrogen. The nanofiber diameter and its distribution were determined and the arithmetic weighted mean together with the corresponding deviation were estimated. The structure of the nanofibers was further analyzed by transmission electron microscopy (TEM, JEM 3000 F, JEOL).

The surface of the ENMs was studied by X-ray photoelectron spectroscopy (XPS, Physical Electronics Spectrometer, PHI 5700) with X-ray Mg Kα radiation (300 W, 15 kV, 1253.6 eV) as excitation source and a multi-channel hemispherical electroanalyzer. High-resolution spectra of C-1s, O-1s, F-1s, S-2p and N-1s in the binding energy range 0-1130 eV were recorded at three take-o angles (15º, 45º and 75º corresponding to the penetration depth of 2.5, 6.8 and 9.3 nm from the top surface of the sample, respectively). The characteristic peaks of oxygen (O-1s) and sulfur (S-2p) atoms of both PSF and FPA were detected at 531 and 167.8 eV, respectively; while the peaks of the binding energy at 685.7 eV and 400.2 eV correspond to fluorine (F-1s) and nitrogen (N-1s) atoms associated only to FPA. Typical XPS diagrams of FPA blended PSF ENMs are shown in Supporting Information (SI) **Figure S2**. Based on the peak intensities, the atomic percentage of each ion was evaluated. The PHI ACCESS ESCA-V6.0F software package was used for data acquisition and analysis.

The thickness (δ) of the ENMs was measured by the micrometer Millitron Phywe (Mahr Feinprüf, type TYP1202IC). The water contact angle (θ) was measured at 23 ± 1 ºC using a computerized optical system CAM100, equipped with a CCD camera, frame grabber and image analysis software CAM200usb. More information can be found elsewhere [44,23,46].

The mechanical properties (Young's modulus, Y_M; tensile strength, T_S; elongation at break, E_b) of the ENMs were studied according to ASTM D 3379-75 specifications using an Instron dynamometer (model 3366) at 23 °C and a cross-head speed of 22 mm/min.

The void volume fraction (ε) of the ENMs was obtained from the measured weights of each sample using isopropyl alcohol (IPA), which penetrates into the inter-fiber space of the ENM and distilled water, which does not enter into the inter-fiber space [46].

The mean size of the inter-fiber space (d_i) and its distribution were determined using a capillary flow porometer (POROLUX^{TM} 100). The followed procedure was described elsewhere [44,46].

The liquid entry pressure (*LEP*), which is the minimum hydrostatic pressure applied on the ENM before liquid penetrates into the inter-fiber space, was measured for distilled water and salt aqueous solutions at different NaCl concentrations (12, 30 and 60 g/L) using the experimental system and following the procedure detailed elsewhere [45,46].

Direct contact membrane distillation (DCMD) experiments were carried out using Lewis cell shown schematically in [23]. In this study, the volume of both the feed and permeate chambers was 0.25 L. the feed and permeate temperatures were maintained at 80ºC and 20ºC, respectively; and both the feed and permeate circulation rates were 500 rpm. Distilled water and aqueous NaCl solutions of different concentrations (12, 30 and 60 g/L) were employed for feed solutions. For each ENM, the DCMD tests were performed for a total period of at least 12 h except for those

membranes that were wet as it will be discussed later on. Longer DCMD tests, 30 h, were carried out for some selected ENMs. The NaCl rejection factor was calculated as $\alpha = (1-C_{b,p}/C_{b,f})\cdot 100$, where $C_{b,f}$ and $C_{b,p}$ are the concentrations of the bulk feed and permeate solutions,

3. Results and discussions

3.1. Morphological structure, elemental composition and superhydrophobic character

Figure 1 shows some representative SEM images of PSF and FPA blended PSF nanofibers and ENMs together with their nanofiber size distributions and TEM images. Bead-free networks of randomly oriented nanofibers were formed. With the increase of the FPA content in the spinning dope, the nanofibers acquired gradually more curved shapes with larger diameters and wider size distributions (**Figure 1** and **Table 1**). This is due to the significant enhancement of the viscosity of the spinning dope (268.2%) with the increase of the FPA amount up to 6 wt % although the electrical conductivity was also increased by 31.8% and the surface tension was decreased by 44.2% (**Table1**). In electrospinning, a higher electrical conductivity induces a higher net charge density carried by the electrified spinning jet and greater Coulombic interactions resulting in more intense stretching of the jet and a smaller fiber diameter. In this case, the viscosity plays a predominant role on the nanofiber size and its distribution.

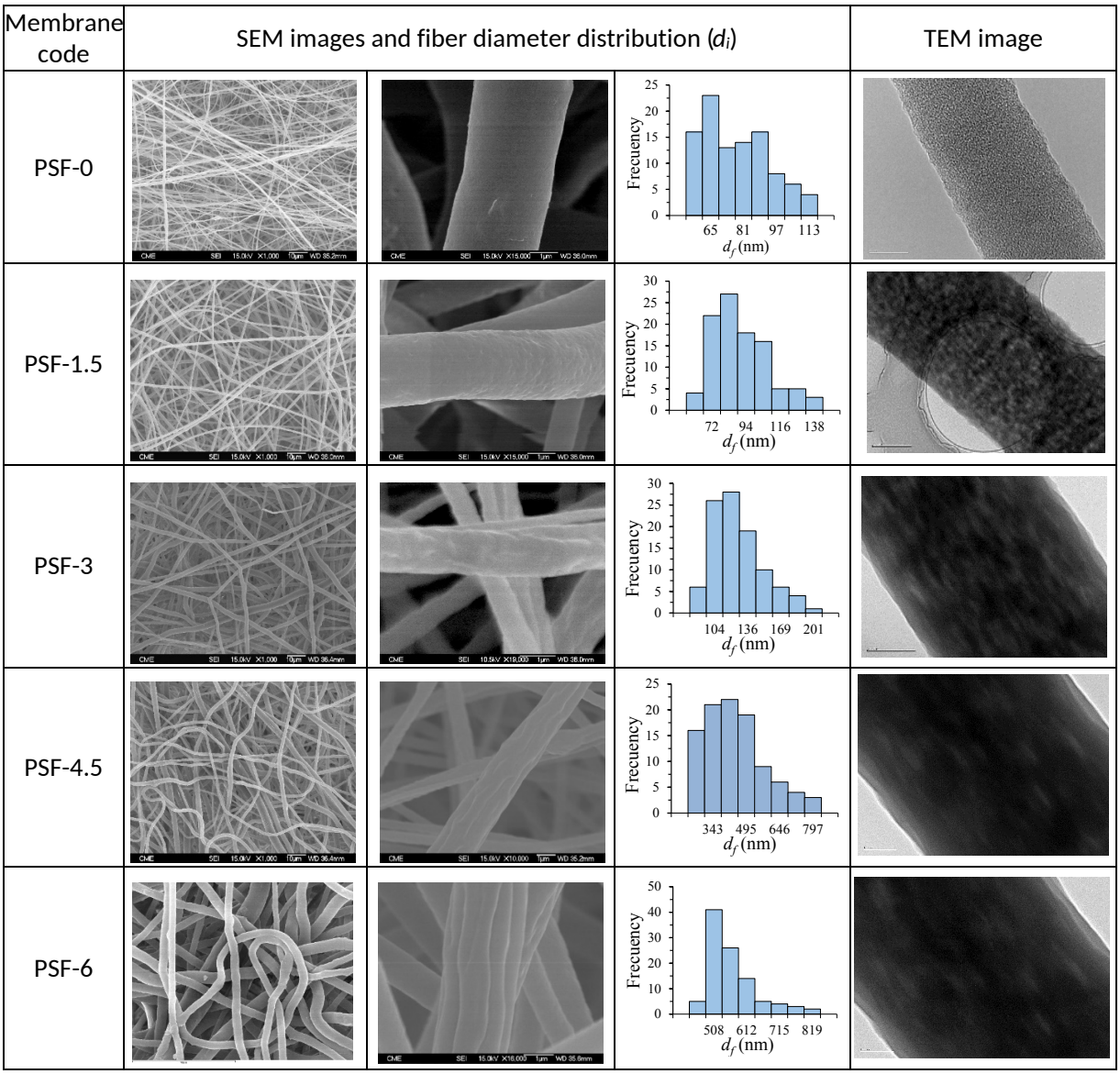

Figure 1. *SEM (left and middle) and TEM (right) images of the PSF and FPA blended PSF ENMs together with their diameter size distribution histograms obtained from SEM images.*

It must be pointed out that even if the surface tension of the dispersion was decreased considerably, it was still high enough to counteract the repulsive forces in the electrified jet preventing the formation of beads. High magnification SEM (**Figure 1** SEM images right) and TEM images showed more clearly the morphological differences between the PSF and the FPA blended PSF

nanofibers. FPA changed the surface of the PSF nanofiber rendering it rougher and corrugated in the direction of the nanofiber axis when the FPA concentration was higher than 1.5 wt % (**Figure 1**). This was not attributed to the shear from the inner surface of the metallic needle; but to the physico-chemical characteristics of the electrospinning dope as will be discussed later on in relation to the FPA segregation to the nanofiber surface. As it is well known, the TEM images show the internal structure of the nanofibers. Compared to the PSF nanofiber, which has a uniform and homogenous structure, the FPA blended PSF nanofibers exhibited a heterogeneous structure as shown by the dark regions in TEM images (**Figure 1**).

The surface elemental composition of the PSF and FPA blended PSF nanofibers was studied by XPS at three take-off angles 15º, 45º and 75º as stated earlier. The results are summarized in **Table 2**. For the PSF nanofiber, with the increase of the take-off angle from 15º to 75º the atomic percentage of oxygen (O-1s) and sulfur (S-2p) was decreased by 8.0 and 23.7%, respectively. This indicates the possible reorientation of PSF polymer chain by the induced electric field between the metallic needle and the collector. In this study, electrospinning was carried out applying a positive polarity voltage. Thus, the electronegative groups of the polymer such as oxygen together with sulfur, which is double bonded with oxygen, would be attracted by the positive charges accumulated at the surface of the electrified liquid jet and electronegative dipoles will be formed at the surface of the nanofiber [47,48]. This means that oxygen double-bonded with sulfur would be reoriented to the nanofiber surface, whereas the hydrophobic isopropylidene group would be positioned away from the surface. Thorough experimental studies must be focused on the effects of the electric field on polymer molecular reorientation by applying both positive and negative polarity voltages and employing other polymers as well.

Table 2. *Atomic percentage of different elements found on the surface of the PSF and FPA blended PSF ENMs using XPS at different take-off angles.*

ENMs	Take-off angle [a] (º)	C-1s (%)	O-1s (%)	F-1s (%)	S-2p (%)	N-1s (%)
PSF-0	15	84.9	11.3	0	3.8	0
	45	86.3	10.7	0	3.0	0
	75	86.7	10.4	0	2.9	0
PSF-1.5	15	62.7	6.6	26.6	1.2	2.9
	45	63.4	6.9	25.6	1.2	3.0
	75	65.6	6.9	22.4	1.5	3.7
PSF-3	15	56.2	6.6	33.5	1.4	2.4
	45	59.0	6.7	30.3	1.2	2.8
	75	66.1	7.5	21.6	1.6	3.2
PSF-4.5	15	52.3	6.5	37.6	1.2	2.3
	45	56.4	6.6	33.4	1.2	2.4
	75	61.6	6.9	27.0	1.3	3.3
PSF-6	15	47.4	5.2	44.0	< 0.1	3.4
	45	51.5	5.8	38.9	< 0.1	3.7
	75	55.5	5.5	35.3	< 0.1	3.7

[a] XPS analysis depth, L_{XPS}, depends on the take-off angle: L_{XPS} (15º) = 2.5 nm; L_{XPS} (45º) = 6.8 nm and L_{XPS} (75º) = 9.3 nm.

The contents of both oxygen and sulfur were reduced considerably in all FPA blended PSF nanofibers from the pristine PSF nanofibers, but no significant changes were detected between the three take-off angles. This indicates that the PSF polymer chains did not have the chance to be

reoriented due to the presence of FPA in the electrospinning dope. Besides, the changes in the atomic percentage of fluorine and nitrogen both associated with the presence of FPA, were clearly detected, i.e. for a given take-off angle, the atomic percentage of fluorine increased with the increase of FPA content in the spinning dope, while that of nitrogen showed minimum at PSF-4.5. In general, for all FPA blended PSF nanofibers, fluorine to carbon ratio decreased gradually with an increase in the take-off angle but it was higher than for pristine PSF, which is equal to zero. It is to be noted that the XPS elemental analysis provided the results considerably different from the theoretical elemental composition of the FPA blended PSF nanofibers (see **Table S1** shown in Supporting Information (SI)), which was calculated based on the molecular structure of FPA (**Table S2**) assuming uniform distribution of FPA in the blended PSF ENMs, i.e. the experimental atomic percentages of F and N are much greater than the calculated ones (up to 24.2 times for F and 10.7 for N). These results confirmed the FPA surface segregation due to its lower surface free energy than that of PSF. The same observations have been made previously for flat-sheet films [21-24,43,49], hollow fibers [19,20], both prepared by the phase inversion process, and electrospun nanofibers [17,33,34], where different types of host hydrophilic polymers and lower surface energy additives were employed. In addition, for electrospun nanofibers an increasing surface fluorine enrichment was observed with the increase of their fiber diameter (see **Tables 1 and 2**). As the fiber diameter increases, the solvent evaporation rate decreases, allowing a longer period for surface segregation before the polymer solidification. Thus, the surface segregation was enhanced as the fiber diameter increased from PSF-1.5 to PSF-6.

The PSF nanofiber surface coverage by FPA was calculated based on the experimental atomic composition of fluorine and the structure of PSF and FPA. Furthermore, FPA was split into PU and fluorohydrocarbon components in the calculation. The results for the PSF-4.5 nanofiber

corresponding to 15º take-off angle were 51.4% fluorohydrocarbon, 12.7% PU and 35.9% PSF, indicating that a substantial part of the membrane surface was covered by FPA and the fluorinated tails of the FPA were protruded at the nanofiber surface while the PU prepolymer was embedded in the host PSF matrix. The observed increase of the fluorine content and the roughness due to the observed corrugated structure at the surface of the nanofiber by the blend of FPA would affect the water contact angle of the nanofibrous mat.

Indeed, the measured water contact angle (θ) was close to or higher than 150º for all prepared FPA blended PSF nanofibrous ENMs as shown in **Figure 2**. The contact angle increased with the increase of the FPA content up to 4.5 wt % and then leveled off, PSF-3, PSF-4.5 and PSF-6 ENMs being superhydrophobic (θ above 150º).

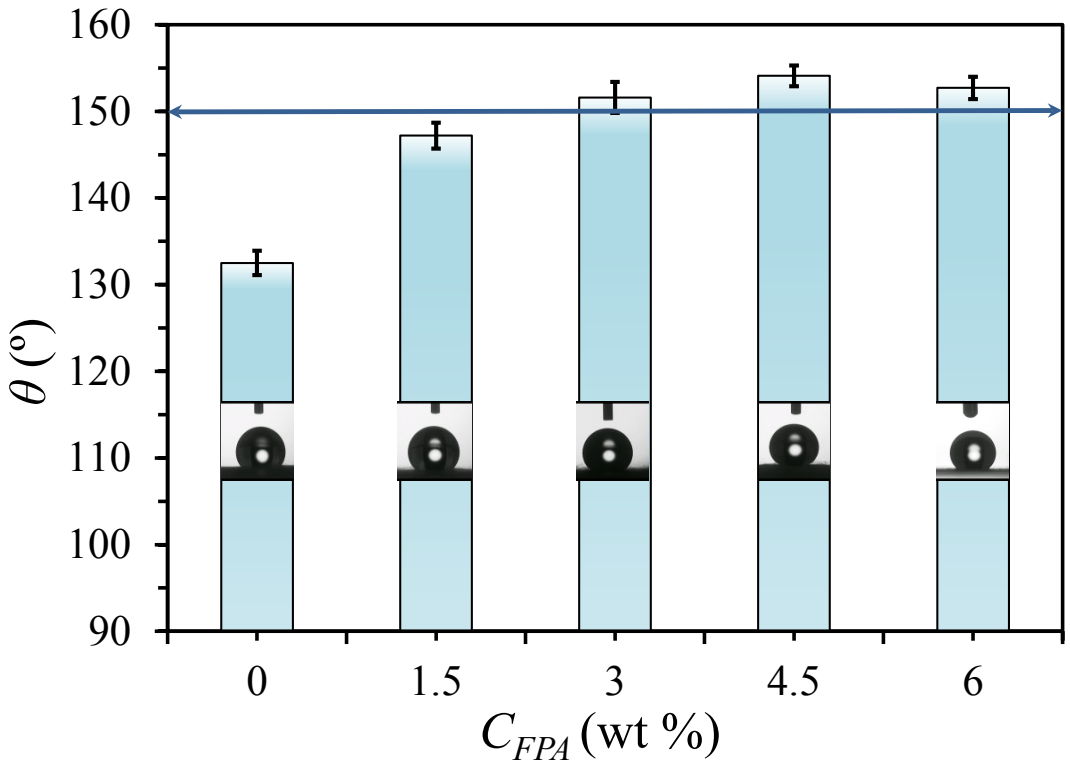

Figure 2. *Water contact angle (θ) of the PSF and FPA blended PSF ENMs as a function of FPA concentrations in the electrospinning dope.*

There are two opposing effects of nanofiber morphology and nanofiber chemistry on the contact angle. 1) As for the surface morphology, the nanofiber diameter becomes larger and the size and number of the air pocket decrease with an increase in FPA content, leading to the decrease in contact angle according to the Cassie and Baxter model [50]. 2) As for the surface chemistry, the hydrophobicity increases with an increase in FPA content, leading to the increase in contact angle. Experimental results show clearly that the effect of the surface chemistry surpasses that of the surface morphology.

3.2. Mechanical properties of the PSF modified ENMs

The tensile behavior of both PSF and FPA blended PSF ENMs were plotted in **Figure 3** and the mechanical properties (Young's modulus, Y_M; tensile strength, T_S and elongation at break, E_b) were summarized in **Table 3**. The Y_M, T_S and E_b values of the PSF ENM were lower than those of the previous study (i.e. Y_M = 47.2 ± 0.6 MPa; T_S = 2.6 ± 0.4 MPa and E_b = 38.5 ± 0.3 %) for PSF ENM [51]. This is attributed mainly to the ENM thickness (**Table 3**) as the PSF ENM prepared in this study is thinner (110 ± 9 µm compared to 564 ± 37 µm of the previous study). As well, electrospinning conditions and time were different. In fact, the effect of electrospinning time on the mechanical properties had been thoroughly investigated, observing higher Y_M and T_S values for thicker polyvinylidene fluoride (PVDF) ENMs [45]. For the MD process, an optimum thickness should exist, as a result of a compromise between its effect on permeability and heat transfer resistance.

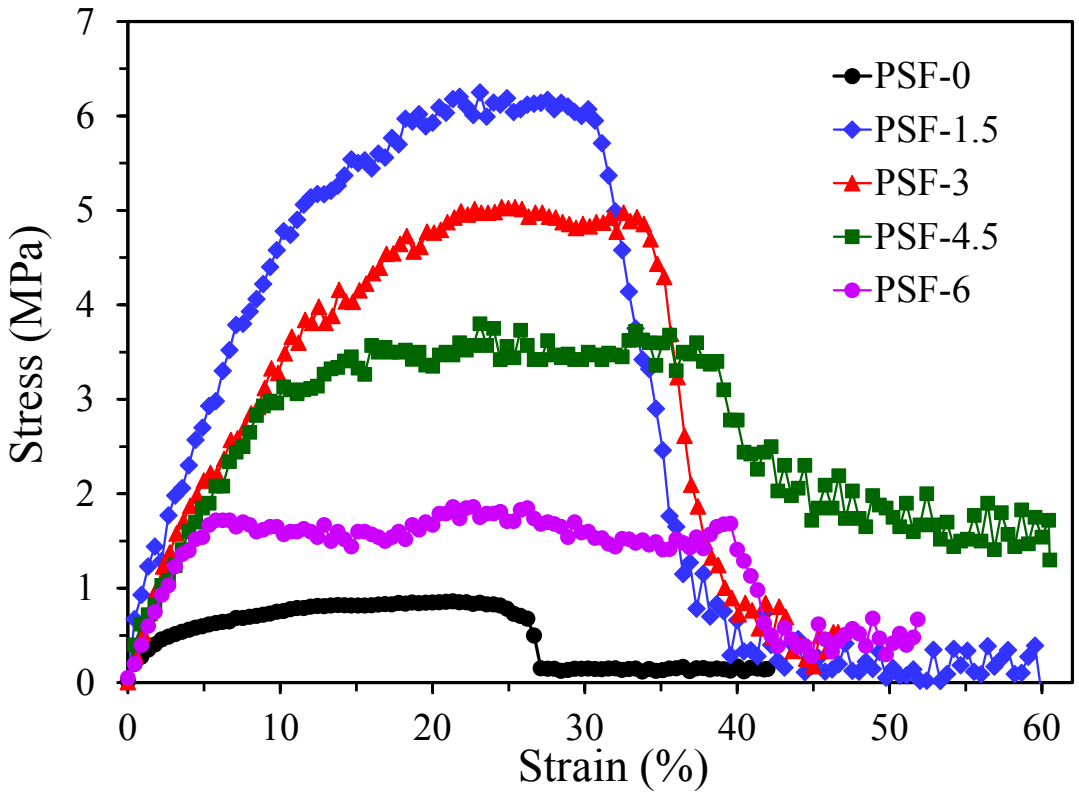

Figure 3. *Stress–strain curves of the PSF and FPA blended PSF ENMs for different FPA concentrations.*

From **Table 3**, all Y_M, T_S and E_b values increased upon addition of FPA indicating the improvement of mechanical strength. However, Y_M, and T_S decreased linearly as the FPA increased with correlation coefficients of 0.9872 and 0.9617, respectively (see **Figure S4**) despite the increase in thickness (i.e. 163.7 % increase from that of PSF-1.5 to PSF-6, see **Table 3**). This is because the curved nanofibers are more poorly aligned (see **Figure 1**), and possess more void spaces (larger void volume fraction, ε, see **Table 3**) as FPA content increases. On the other hand, E_b increased linearly with an increase in FPA content with a correlation coefficient of 0.9978 (see **Figure S4**). This is mainly due to the increase of the nanofiber diameter and the ENM thickness.

Table 3. *Mechanical properties (Young's modulus, Y_M; tensile strength, T_S; elongation at break, E_b), thickness (δ), void volume fraction (ε) and mean inter-fiber space (d_i) of the PSF and FPA blended PSF ENMs.*

ENMs	Y_M (MPa)	T_S (MPa)	E_b (%)	δ (μm)	ε (%)	d_i (nm)
PSF-0	14.3 ± 1.4	0.85 ±0.03	21.9 ± 0.5	110 ± 9	82.3 ± 0.7	2748 ± 69
PSF-1.5	65.0 ± 0.8	6.0 ± 0.4	31.1 ± 1.6	111 ± 11	84.1 ± 0.2	868 ± 21
PSF-3	52 ± 3	4.4 ± 0.4	34.3 ± 0.8	129 ± 12	87.1 ± 0.8	932 ± 21
PSF-4.5	47 ± 4	3.73 ± 0.24	36.7 ± 1.1	194 ± 21	95.4 ± 0.3	1388 ± 48
PSF-6	32 ± 3	1.48 ± 0.23	39.4 ± 0.3	293 ± 100	97.9 ± 0.2	2011 ± 25

As it is well known, compared to the membranes used in pressure-driven processes (reverse osmosis, RO; nanofiltration, NF, ultrafiltration, UF and microfiltration, MF) MD does not require membranes of good mechanical properties since the transmembrane pressure difference is almost nil. However, the mechanical strength of MD membranes should be high enough to be packed in the module. It should be noted that the FPA blended PSF ENMs proposed in the present study for MD exhibited better Y_M values (i.e. more than 4 times greater) than the superhydrophobic PVDF/SiO_2 surface modified [52] and mixed matrix [53] ENMs used in desalination by DCMD and VMD, respectively.

3.3. Void volume fraction, Inter-fiber space and liquid entry pressure of PSF and FPA blended PSF ENMs

As can be seen in **Table 3**, with the increase of the FPA concentration in the PSF host polymer solution the void volume fraction (ε) was increased in contrast to what it was expected taking into consideration the gradual increase of the electrical conductivity of the polymer solution up to 31.8% (**Table 1**). In fact, a greater electrical conductivity of the electrospinning solution results in a better dissipation of electric charges to the collector, less repulsive forces between nanofibers and a more compact fibrous web as the consequence. The observed opposite result may be attributed to the increase of the fiber diameter and thickness of the ENM associated principally to the enhanced viscosity of the polymer solution up to 268.2% (**Table 1**). With the increase of the thickness, the distance between the needle and the collector was reduced slightly and the formed layer of the ENM acted as an insulator towards the dissipation of electric charges towards the collector (i.e. more electric charges accumulated in nanofibers) leading to more repulsive forces between them and consequently to a less packed nanofibrous web with a higher void volume fraction. In fact, Essalhi and Khayet [45] reported that the void volume fraction was not uniform throughout the nanofibrous web thickness. It is worth quoting that among other superhydrophobic ENMs proposed for MD, PSF-4.5 and PSF-6 exhibited the highest ε values (**Table 4**).

For the FPA blended PSF ENMs, an enhancement of the inter-fiber space (d_i) with the increase of FPA content was observed according to the increase of the void volume fraction (**Table 3**). As can be seen from the data given in **Table 4**, the d_i values of the FPA blended PSF ENMs were within the d_i range of other superphydrophobic ENMs (0.18 - 2.82 μm). It is to be noted that in this study no hot-press step was applied to the prepared ENMs after electrospinning. The cumulative and differential distributions of the inter-fiber space of the PSF and FPA blended PSF ENMs were

plotted in **Figure 4**. The size distribution curves of the FPA/PSF blend ENMs shifted to the left of the PSF ENM curve. Other than the change of the properties of the polymer solution, this is also due to the FPA segregation to the surface of the PSF nanofiber as discussed in section 3.1.

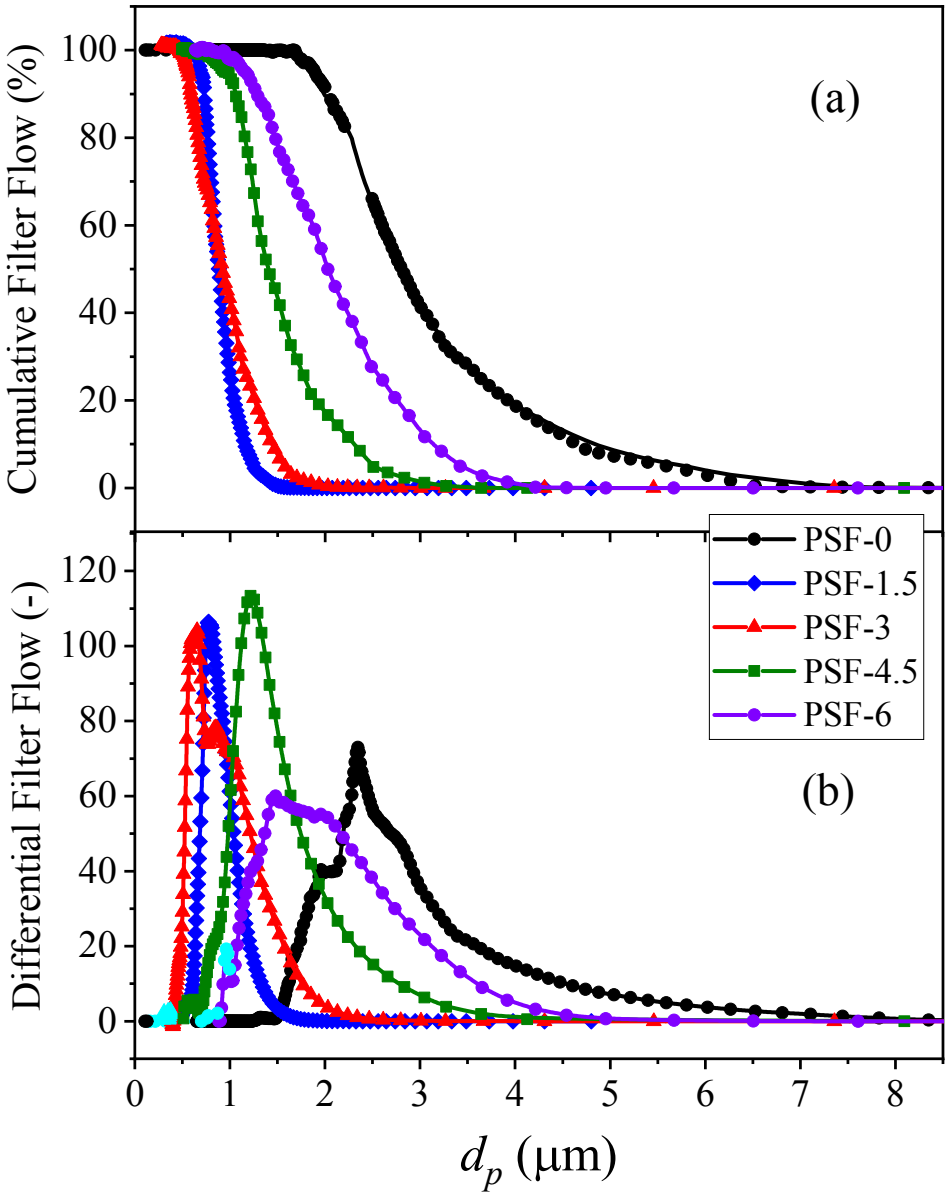

Figure 4. Cumulative (a) and differential (b) filter flow distributions of the inter-fiber space of the PSF and FPA blended PSF ENMs for different FPA concentrations.

Upon addition of FPA, the maximum d_i decreased significantly (see Supporting Information (SI) **Figure S5**). Together with the increase in contact angle (**Figure 2**), liquid entry pressure (*LEP*) of PSF-1.5 is far more than PSF-0 for all tested liquids, including distilled water, 12, 30 and 60 g/L of NaCl aqueous solutions (**Figure 5**). However, as can be seen in **Figure S5** the maximum inter-fiber space ($d_{i,max}$) value was increased with the increase of the FPA concentration, from PSF-1.5 to PSF-6 ENMs, reducing the *LEP* values despite the increase of the water contact angle as indicated by Laplace Equation [46].

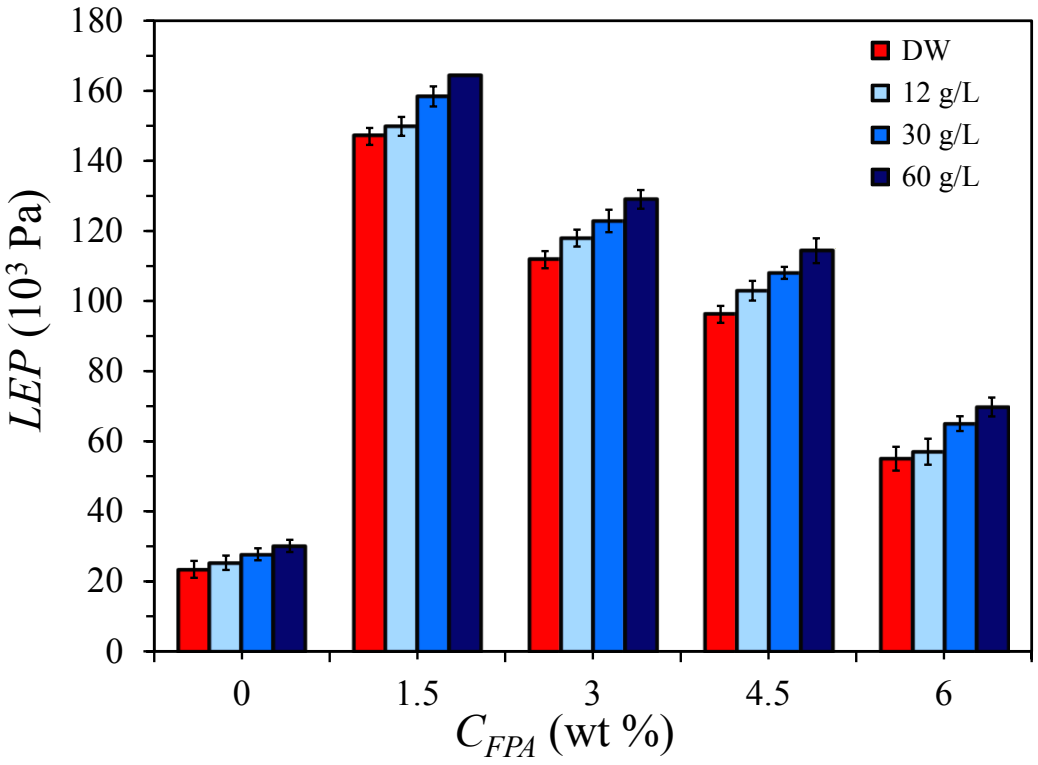

Figure 5. *Liquid entry pressure (LEP) of distilled water and salt (NaCl) aqueous solutions (12, 30 and 60 g/L) of PSF and FPA blended PSF ENMs for different FPA concentrations in the electrospinning dope.*

It should also be noted in **Figure 5** that the *LEP* increases as NaCl concentration increases, which is due to the increase in surface tension with an increase in NaCl concentration, as observed for

other ENMs [51]. It is worth quoting that the *LEP* values of the FPA blended PSF ENMs were within the range of most superhydrophobic modified nanofibrous membranes (0.7 – 3.73 10^5 Pa, **Table 4**).

3.4. DCMD performance of PSF and FPA blended PSF ENMs

The PSF and FPA blended PSF ENMs were considered for desalination by DCMD. The obtained permeate fluxes (*J*) together with the NaCl rejection factors were plotted in **Figure 6a**. After only 2 h DCMD operation, the permeate NaCl concentration of the ENM PSF-0 showed a considerable increase for all tested feeds (i.e. the permeate electrical conductivity increased from 6.097 to 1168.1 µS/cm, 5.485 to 1566.4 µS/cm and 6.319 to 5234.9 µS/cm in a permeate volume of 0.25 L for 12, 30 and 60 g/L NaCl aqueous solutions, respectively, **Figure 6b**). This was due to its very low *LEP* values (i.e. < 30.1 kPa, **Figure 5**) although its θ value was quite high (132.5 ± 1.4º). Besides, the measured permeate flux of the PSF-0 ENM was greater than that of the FPA blended PSF ENMs (i.e. 79.3, 81.1, 79.5 and 87.8 kg/m^2.h for distilled water, 12, 30 and 60 g/L NaCl aqueous solutions, respectively). These fluctuations of the obtained permeate flux was also a proof of the inter-fiber wetting of PSF-0. Therefore, the PSF ENM was not suitable for MD desalination.

The obtained NaCl rejection factors of the PSF-1.5, PSF-3 and PSF-4.5 ENMs were higher than 99.99% and their permeate fluxes were in the range 36.2 – 62.9 kg/m^2.h (**Figure 6a**). For a higher NaCl concentration in the feed aqueous solution, the permeate flux of these ENMs was lower because of the reduction of the water vapor pressure with the NaCl concentration and the e ect of the concentration polarization [46]. Among the electrospun FPA blended PSF ENMs, the PSF-6 ENM showed less NaCl rejection factors (i.e. 97.97, 98.67 and 95.46% for 12, 30 and 60 g/L NaCl

aqueous solutions, respectively). A considerable increase of the electrical conductivity of the permeate with time was registered for the three NaCl aqueous solutions (i.e. from 3.7 to 1206.1 µS/cm, 4.1 to 1683.8 µS/cm and 6.1 to 11517.3 µS/cm for 12, 30 and 60 g/L NaCl aqueous solutions, respectively, **Figure 6b**).

An enhancement of the permeate flux was observed with the increase of the FPA amount in PSF solution up to 4.5 wt %. This was attributed to the increase of both the void volume fraction and inter-fiber space with the increase of the FPA content in PSF host solution as discussed previously although the thickness was also increased (**Table 3**), and to the change of the structure of the ENMs discussed in section 3.1 (i.e. rougher and corrugated nanofiber surfaces attributed mainly to FPA segregation to the nanofiber surface and more curved nanofibrous structure presented in **Figure 1**). Besides, the increase of the permeate flux was due partly to the apparent increase of the ratio of the mean electrospun nanofiber diameter to the inter-fiber space (d_f/d_i) that induced more Knudsen mass transport contribution (i.e. more collisions between the water vapor molecules and nanofiber) rather than Brownian molecular diffusion (i.e. d_f/d_i = 0.105, 0.135 and 0.316 for PSF-1.5, PSF-3 and PSF-4.5, respectively) [60]. In DCMD, water vapor transport through an ENM can be carried out by means of Knudsen type of flow (i.e. for high probability of collisions between water vapor molecules and nanofibers), viscous or Poisseuille type of flow (i.e. for high probability of collisions between water vapor molecules and each other`s) and Brownian molecular diffusion type of flow (i.e. when water vapor molecules transfer through air present in the void volume of the ENM) [46]. In this study, viscous type of flow was negligible as the hydrostatic pressure of both the feed and permeate chambers of the DCMD set-up were maintained at atmospheric pressure.

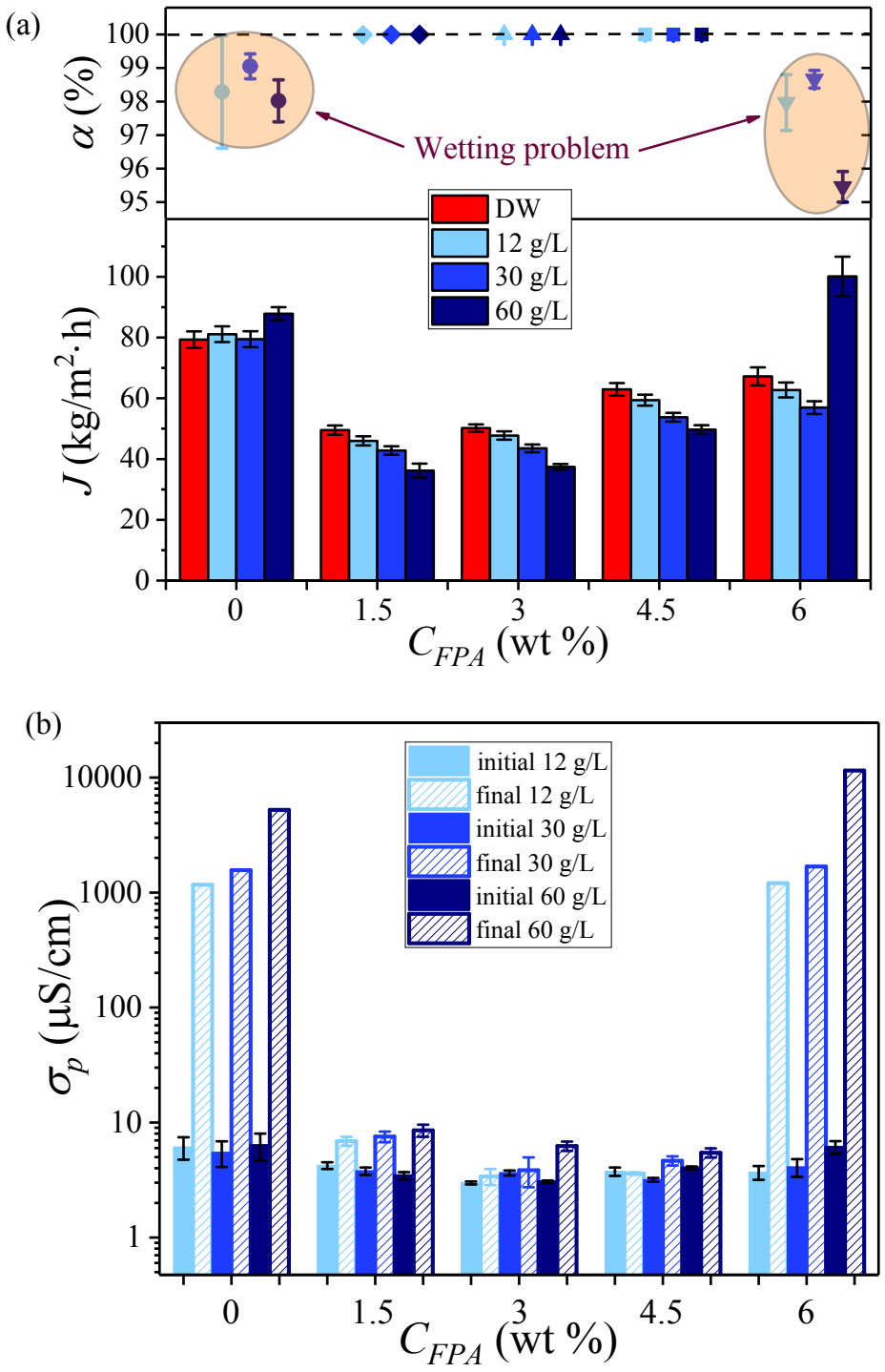

Figure 6. *(a) Permeate flux (J) and NaCl rejection factor ($\alpha = (1-C_{b,p}/C_{b,f})\cdot 100$, where $C_{b,f}$ and $C_{b,p}$ are the concentrations of the bulk feed and permeate solutions, respectively), and (b) Initial (I) and final (F) electrical conductivity (σ_p) of the permeate of the PSF and FPA blended PSF ENMs as a function of FPA concentration and for different salt aqueous solutions as feed.*

Because of their better DCMD desalination performance, the two ENMs PSF-3 and PSF-4.5 were selected for a period of 30 and 32 h DCMD desalination (30 g/L NaCl aqueous feed solution, 4 consecutive days stopping the tests overnights), respectively. The registered data were plotted in **Figure 7**. For both ENMs stable permeate fluxes and permeate concentrations were registered over the mentioned DCMD testing period. For the PSF-3 ENM the permeate flux was 42.9 ± 0.4 kg/m^2.h and its electrical conductivity was in the range 4.0 – 4.7 μS/cm with a mean value of 4.1 ± 0.2 μS/cm. The permeate flux of the PSF-4.5 ENM was 53.8 ± 0.2 kg/m^2.h and its electrical conductivity was in the range 4.1 – 5.1 μS/cm being the mean value 4.6 ± 0.3 μS/cm). The absence of a continuous increase of the electrical conductivity of the permeate for both ENMs proved their suitability for DCMD desalination. Compared to the PSF-3 ENM, the higher permeate flux of the PSF-4.5 ENM (25.4%) is due to its greater void volume fraction (9.5%) and inter-fiber space (48.9%) as well as to its rougher and corrugated nanofiber surface that may reduce both the temperature and concentration polarization phenomenon although it was 50.4% thicker (**Figure 1**, **Table 3**).

Compared to the surface modified superhydrophobic ENMs proposed for MD desalination (**Table 4**), the FPA blended PSF ENMs, PSF-3 and PSF-4.5, exhibited competitive DCMD performance in spite of being thicker. This is attributed to their relatively larger inter-fiber space and void volume fraction. It is worth quoting that other than the ENMs presented in Table 4 the superhydrophobic ENMs claimed to have the highest permeate fluxes were the unmodified polysterene (PS) superhydrophobic ENMs (i.e. 25 wt % PS in *N*,*N*-dimethyl formamide (DMF), supported on polyethylene terephthalate (PET), 104.8 ± 4.9 kg/m^2.h, DCMD, 10 h, 70/20ºC, 20 g/L NaCl) with a low permeate electrical conductivity (≈ 2.5 μS/cm) [61], the fluorinated polyxadiazole (F-POD, 18 wt% in N-methyl pyrrolidone, NMP, 78 kg/m^2.h, DCMD short-term

test, 80/22ºC, Red sea) and the fluorinated polytriazole (F-PT, 18 wt% in NMP, 85 kg/m^2.h, DCMD short-term test 80/22ºC, Red sea) both with smaller NaCl rejection factors as low as 99.95% [62].

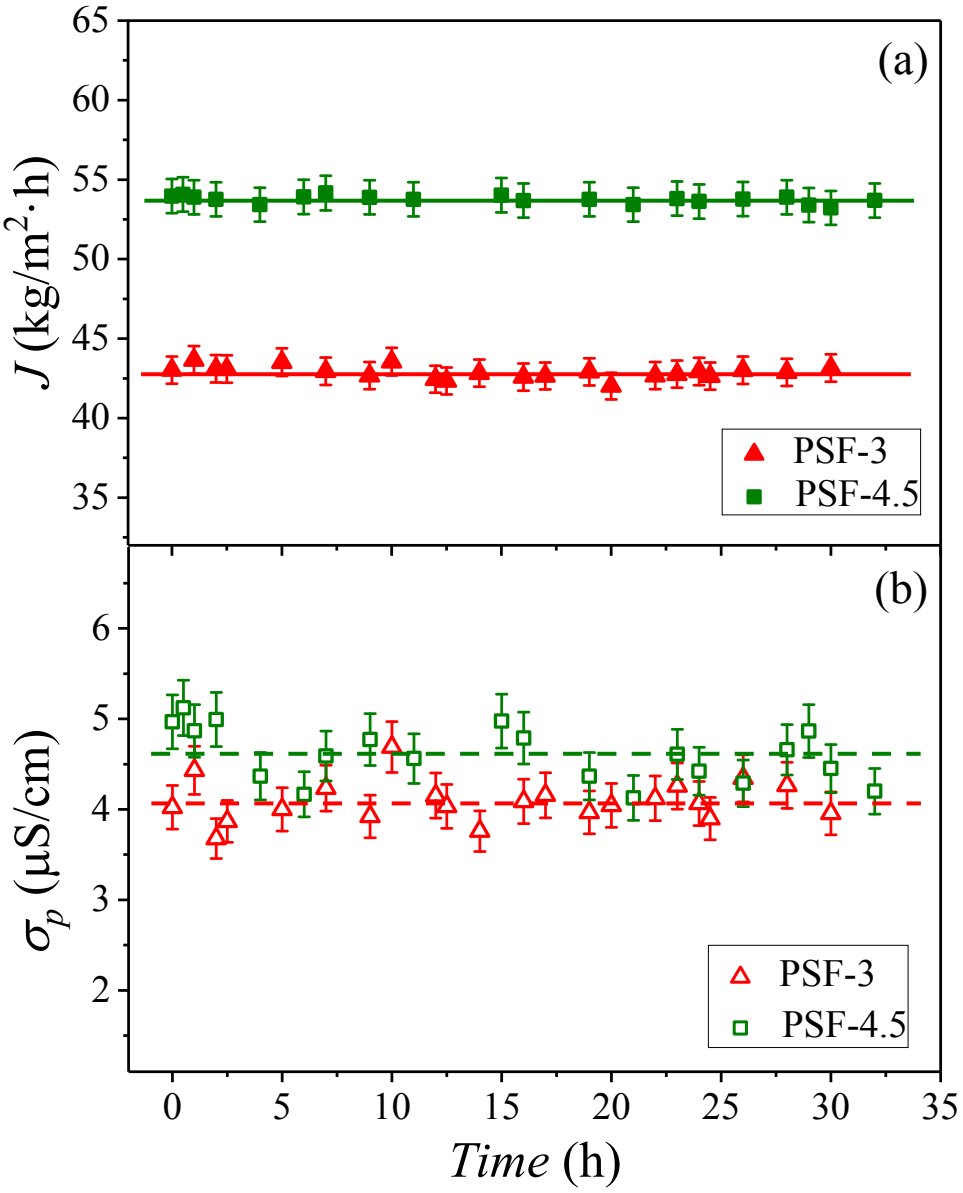

Figure 7. *Permeate flux (a) of PSF-3 and PSF-4.5 and their electrical conductivities (b) as a function of DCMD operation time (30 g/L NaCl aqueous solution as feed, T_f = 80ºC, T_p = 20°C, stirring rate 500 rpm).*

Table 4. Characteristics and MD performance of surface modified superhydrophobic ENMs proposed for desalination.

Material [a]	θ (º)	*LEP* (10^5 Pa)	d_i (µm)	ε (%)	δ (µm)	*J* (kg/m².h)	σ_p (µS/cm) / (α, %)	Ref.
200% FS-SiO_2/PVDF 3 wt % PVDF	154.0	1.5 *	0.32	78.5 *	72	25 (DCMD, 25 h, 60/20ºC, 3.5 g/L NaCl)	< 5 (>99.99%)	[54]
200% FS-SiO_2/PVDF 5 wt % PVDF	150	1.8 *	0.36	65 *	76	21 (DCMD, 40 h, 60/20ºC, 3.5 g/L NaCl)	< 5 (>99.99%)	[54]
200% FS-SiO_2/PVDF 5 wt % PVDF	156 ± 2	1.79 ± 0.07	0.77 ± 0.02	83 ± 1	129 ± 8	18.9 (DCMD, 50 h, 60/20ºC, 3.5 g/L NaCl)	< 5	[55]
Ag/PDA/PVDF [b]	153 ± 4	1.46 ± 0.12	0.34 ± 0.01	77 ± 1	47 ± 4	31.6 (DCMD, 8 h, 60/20ºC, 35 g/L NaCl)	< 5	[56]
5% CNT/PVDF-HFP	158.5	0.99	0.29	84 ± 1	81	29.5 (DCMD, 5 h, 60/20ºC, 35 g/L NaCl)	< 1 (99.99%)	[57]
PVDF-HPF/PAN (25/75)	150	0.94	1	90	82	30 (DCMD, 3 h, 60/20ºC, 35 g/L NaCl)	(> 98.5%)	[58]
334 % M-SiO_2/PVDF	152 ± 1	1.64 ± 0.11	0.23	79	173 ± 8	25 (DCMD, 100 h, 60/15ºC, 35 g/L NaCl)	< 5	[52]
2 wt % FAS grafted PVA (10 wt % PVA)	158 ± 2	1.79 ± 0.03	0.46 ± 0.01	82 ± 2	100 ± 3	25.2 (VMD, 16 h, 60ºC, 9 kPa, 35 g/L)	< 5	[9]
PPFDA/ PA6(3)T [c]	151 ± 2	3.73	-	69	55 ± 2	11 (AGMD, 3 h, 70/25ºC, 35 g/L)	(99.99%)	[13]
OTFE/PVDF-HFP	156 ± 2	2.4 – 2.8	0.18 – 0.22	60	125 ± 25	13-14 (DCMD, 3 h, 67/25ºC, 20 g/L)	130 (99.9%)	[59]

PDMS/PSF (1 g in hexane, 23 wt % PSF)	151.1 ± 1.1	0.7	2.819	82	97 ± 5	21.5 (DCMD, 12 h, 70/20ºC, 30 g/L)	4.224 - 4.523	[42]
PSF-3	151.6 ± 1.8	1.23 ± 0.03 [d]	0.932 ± 0.021	87.1 ± 0.8	129 ± 12	42.88 ± 0.39 (DCMD, 30 h, 80/20ºC, 30 g/L) 29.89 ± 0.15 (DCMD, 3 h, 65/20ºC, 30 g/L)	4.1 ± 0.2 3.9 – 4.3	This study
PSF-4.5	154.1 ±1.2	1.08 ±0.02 [d]	1.388 ± 0.048	95.4 ± 0.3	194 ± 21	53.76 ± 0.24 (DCMD, 32 h, 80/20ºC, 30 g/L) 33.47 ± 0.18 (DCMD, 3 h, 65/20ºC, 30 g/L)	4.6 ± 0.3 4.5 – 4.7	This study

* Values estimated from the given figure

[a] For filled ENMs, the concentration of filler is based on the polymer weight

[b] Multi-step modification procedure

[c] PA6(3)T ENM coated by PPFDA using initiated chemical vapor deposition (iCVD)

[d] For 30 g/L NaCl solution

Abbreviations: PVDF (polyvinylidene fluoride), PVDF-HFP (polyvinylidene fluoride-hexafluoropropylene), PAN (polyacrylonitrile), PVA (poly(vinyl alcohol)), PDMS (polydimethylsiloxane), PSF (polysulfone), PDA (poly-dopamine), FAS (fluoroalkylsilane), PPFDA (poly(1H,1H,2H,2H-perfluorodecyl acrylate)), PA6(3)T (poly(trimethyl hexamethylene terephthalamide)), OTFE (tetrafluoroethylene oligomers), FS-SiO_2 (modified silica by α,ω-triethoxysilane-terminated perfluoropolyether ($(EtO)_3Si$-PFPE$Si(OEt)_3$), M-SiO_2 (modified SiO_2 by octamethylcyclotetrasiloxane, AEROSIL R106), Ag (silver nanoparticle), CNT (carbon nanotube), DCMD (direct contact membrane distillation), VMD (vacuum membrane distillation), AGMD (air gap membrane distillation).

4. Conclusions

Very few research studies have been carried out on the in situ surface modification of electrospun nanofibers. In this study, superhydrophobic and bead-free electrospun nanofibers were successfully prepared using a blend of a host hydrophilic polymer, polysulfone (PSF), and a small amount of an oligomeric fluorinated polyurethane additive (FPA), i.e. at least 3 wt % FPA in the PSF blend. During electrospinning, a spontaneous FPA segregation to the nanofiber surface was detected by means of X-ray photoelectron spectroscopy (XPS) at different take-off angles.

The addition of FPA rendered the nanofibers heterogeneous with rougher and corrugated surfaces in the direction of the nanofiber axis attributed mainly to FPA segregation to the nanofiber surface. These affected not only the hydrophobic character of the ENMs but also their inter-fiber space, liquid-entry pressure (*LEP*), fiber size, void volume fraction and mechanical properties.

The increase of the FPA amount in the PSF blend resulted in nanofibers with bigger diameters and wider diameter distributions due to the considerable enhancement of the viscosity of the electrospinning dope although its electrical conductivity was increased and the surface tension was decreased. Compared to PSF ENM, improved mechanical properties were achieved for the FPA blended PSF ENMs. With the increase of the FPA concentration in the PSF host polymer solution both the void volume fraction and the inter-fiber space were increased. The *LEP* was higher for the FPA blended PSF ENMs compared to that of PSF ENM (PSF-0) but it decreased with the increase of the FPA amount in the PSF host polymer solution although the water contact angle was enhanced reaching values greater than 150º. This was due to the increase of the maximum size of the inter-fiber space.

The FPA blended PSF ENMs prepared with FPA amounts up to 4.5 wt % (PSF-1.5, PSF-3 and PSF-4.5) proved to be adequate for desalination by direct contact membrane distillation (DCMD) with competitive and stable permeate fluxes. For example, by the ENM prepared with 4.5 wt% FPA in the PSF blend (PSF-4.5), a permeate flux of 53.8 kg/m^{2}h was achieved at a feed temperature of 80ºC and a permeate temperature of 20ºC, when 30 g/L NaCl feed aqueous solution was treated by DCMD. The electrical conductivities of the permeate were very low (< 5.1 μS/cm) with extremely high rejection factors (> 99.99%). No inter-fiber space wetting was detected during DCMD desalination for these ENMs. However, PSF and PSF-6 ENMs were found to be inappropriate for DCMD application because of their low *LEP* values.

ASSOCIATED CONTENT

Supporting Information

Synthesis, chemical structure and characteristics of the used fluorinated polyurethane additive (FPA) (**Figure S1**), typical XPS diagrams of FPA/PSF blended ENMs at a take-off angle of 15º, which corresponds to 2.5 nm from the top surface of the samples (**Figure S2**), theoretical atomic composition of PSF and FPA blended PSF ENMs (**Table S1**), atomic composition of FPA (**Table S2**), water contact angle (θ) vs. fiber diameter (d_f) of the PSF and FPA blended PSF ENMs (**Figure S3**), Y_M , T_S and E_b as a function of the FPA amount in the PSF electrospinning solution (**Figure S4**), maximum, mean and minimum size of the inter-fiber space (d_i) of the PSF and FPA blended PSF ENMs (**Figure S5**).

ORCID

Mohamed Khayet: 0000-0002-5117-2975

Carmen García-Payo: 0000-0002-6809-3907

Acknowledgments

The authors gratefully acknowledge the financial support of the Ministry of Economy and Competitiveness (MEC) (CTM2015-65348-C2-2-R) and are thankful to Dr. M. Essalhi for his help in preparation and characterization of some nanofibrous masts.

5. References

[1] A. Greiner, J.H. Wendor , Electrospinning: A Fascinating Method for the Preparation of Ultrathin Fibers. Angew. Chem., Int. Ed. 46 (2007) 5670.

[2] W. Cui, Y. Zhou, J. Chang, Electrospun Nanofibrous Materials for Tissue Engineering and Drug Delivery. J. Sci. Technol. Adv. Mater. 11(1) (2010) 014108.

[3] X.F. Lu, C. Wang, Y. Wei, One-Dimensional Composite Nanomaterials: Synthesis by Electrospinning and Their Applications. Small 5 (2009) 2349.

[4] B. Ding, M.R. Wang, J.Y. Yu, G. Sun, Gas Sensors Based on Electrospun Nanofibers. Sensors 9 (2009) 1609.

[5] Y. Liao, C.H. Loh, M. Tian, R. Wang, A.G. Fane, Progress in Electrospun Polymeric Nanofibrous Membranes for Water Treatment: Fabrication, Modification and Applications. Progress Polym. Sci. 77 (2018) 69-94.

[6] D.W. Han, A.J. Steckl, Superhydrophobic and Oleophobic Fibers by Coaxial Electrospinning, Langmuir 25 (2009) 9454.

[7] L. Chen, L. Bromberg, J.A. Lee, H. Zhang, H. Schreuder-Gibson, P. Gibson, J. Walker, P.T. Hammond, T.A. Hatton, G.C. Rutledge, Multifunctional Electrospun Fabrics Via Layer-By-Layer Electrostatic Assembly for Chemical and Biological Protection, Chem. Mater. 22 (2010) 1429-1436.

[8] X.Y. Wang, Y.G. Kim, C. Drew, B.C. Ku, J. Kumar, L.A. Samuelson, Electrostatic Assembly of Conjugated Polymer Thin Layers on Electrospun Nanofibrous Membranes for Biosensors, Nano Lett. 4 (2004) 331-334.

[9] Z.Q. Dong, B.J. Wang, X.H. Ma, Y.M. Wei, Z.L. Lu, FAS Grafted Electrospun Poly (Vinyl Alcohol) Nanofiber Membranes with Robust Superhydrophobicity for Membrane Distillation, ACS Appl. Mater. Interfaces 7 (2015) 22652–22659.

[10] Q.F. Wei, W.D. Gao, D.Y. Hou, X.Q. Wang, Surface Modification of Polymer Nanofibers by Plasma Treatment, Appl. Surf. Sci. 245 (2005) 16-20.

[11] S. Kaur, Z. Ma, R. Gopal, G. Singh, S. Ramakrishna, T. Matsuura, Plasma-Induced Graft Copolymerization of Poly(Methacrylic Acid) on Electrospun Poly(Vinylidene Fluoride) Nanofiber Membrane, Langmuir 23 (2007) 13085-13092.

[12] Z. Ma, M. Kotaki, S. Ramakrishna, Surface Modified Nonwoven Polysulphone (PSU) Fiber Mesh by Electrospinning: A Novel Affinity Membrane, J. Membr. Sci. 272 (2006) 179-187.

[13] F. Guo, A. Servi, A. Liu, K.K. Gleason, G.C. Rutledge, Desalination by Membrane Distillation Using Electrospun Polyamide Fber Membranes with Surface Fuorination by Chemical Vapor Deposition, ACS Appl. Mater. Interfaces 7 (2015) 8225–8232.

[14] N.J. Pinto, P. Carrion, J.X. Quinones, Electroless Deposition of Nickel on Electrospun Fibers of 2-Acrylamido-2-Methyl-1-Propanesulfonic Acid Doped Polyaniline, Mater. Sci. Eng. A 366 (2004) 1-5.

[15] M.L. Ma, Y. Mao, M. Gupta, K.K. Gleason, G.C. Rutledge, Superhydrophobic Fabircs Produced by Electrospinning and Chemical Vapour Deposition, Macromolecules 38 (2005) 9742-9748.

[16] M.L. Ma, M. Gupta, Z. Li, L. Zhai, K.K. Gleason, R.E. Cohen, M.F. Rubner, G.C. Rutledge, Decorated Electrospun Fibers Exhibiting Superhydrophobicity, Adv. Mater. 19 (2007) 255-259.

[17] S.J. Hardman, N. Muhamad-Sarih, H.J. Riggs, R.L. Thompson, J. Rigby, W.N.A. Bergius, L.R. Hutchings, Electrospinning Supherhydrophobic Fibers Using Surface Segregating End-Functionalized Polymer Additives, Macromolecules 44 (2011) 6461-6470.

[18] S. Kaura, D. Rana, T. Matsuura, S. Sundarrajan, S. Ramakrishna, Preparation and characterization of surface modified electrospun membranes for higher filtration flux, J. Membr. Sci. 390-391 (2012) 235-242.

[19] Gh. Bakeri, T. Matsuura, A.F. Ismail, D. Rana, A Novel Surface Modified Polyetherimidehollow Fiber Membrane for Gas–Liquid Contacting Processes. Sep. Purif. Technol. 89 (2012) 160-170.

[20] K.C. Khulbe, C.Y. Feng, T. Matsuura, D.C. Mosqueda-Jimenez, M. Rafat, D. Kingston, R.M. Narbaitz, M. Khayet, Characterization of Surface-Modified Hollow Fiber Polyethersulfone Membranes Prepared at Different Air Gaps, J. Appl. Polym. Sci. 104 (2007) 710–721.

[21] M. Qtaishat, D. Rana, T. Matsuura, M. Khayet, Effect of Surface Modifying Macromolecules Stoichiometric Ratio on Composite Hydrophobic/Hydrophilic Membranes Characteristics and Performance in Direct Contact Membrane Distillation, AIChE J. 55 (2009) 3145–3151.

[22] D.E. Suk, T. Matsuura, H.B. Park, Y.M. Lee, Synthesis of a New Type of Surface Modifying Macromolecules (Nsmm) and Characterization and Testing of Nsmm Blended Membranes for Membrane Distillation, J. Membr. Sci. 277 (2006) 177–185.

[23] M. Essalhi, M. Khayet Surface Segregation of Fluorinated Modifying Macromolecule for Hydrophobic/Hydrophilic Membrane Preparation and Application in Air Gap and Direct Contact Membrane Distillation, J. Membr. Sci. 417-418 (2012) 163-173.

[24] M. Qtaishat, M. Khayet, T. Matsuura, Novel Porous Composite Hydrophobic/Hydrophilic Polysulfone Membranes for Desalination by Direct Contact Membrane Distillation, J. Membr. Sci. 341 (2009) 139–148.

[25] Y.H. Lin, K.H. Liao, C.K. Huang, N.K. Chou, S.S. Wang, S.H. Chu, K.H. Hsieh, Superhydrophobic Films of UV-Curable Fluorinated Epoxy Acrylate Resins, Polymer Inter. 59(9) (2010) 1205-1211.

[26] L. Wang, J.Y. Liang, L. He, Superhydrophobic and Oleophobic Surface from Fluoropolymer-SiO2 Hybrid Nanocomposites, J. Colloid Interface Sci. 435 (2014) 75-82.

[27] G.F. Zhang, Q.H. Zhang, Q.Y. Wang, X.L. Zhan, F.Q. Chen, Synthesis and Properties of Gradient Copolymers of Butyl Methacrylate and Fluorinated Acrylate via RAFT Miniemulsion Copolymerizations, J. Appl. Poly. Sci. 133(5) (2016) 42936.

[28] L. Cai, L. Dai, Y.H. Yuan, A.Q. Liu, Z.X. Li, Synthesis of Novel Polymethacrylates with Siloxyl Bridging Perfluoroalkyl Side-Chains for Hydrophobic Application on Cotton Fabrics, Appl. Surf. Sci. 371 (2016) 453-467.

[29] C.A. Bonino, K. Efimenko, S.I. Jeong, M.D. Krebs, E. Alsberg, S.A. Khan, Three-Dimensional Electrospun Alginate Nanofiber Mats via Tailored Charge Repulsions, Small 8(12) (2012) 1928-1936.

[30] X.Y. Sun, R. Shankar, H.G. Börner, T.K. Ghosh, R.J. Spontak, Field-Driven Biofunctinoalization of Polymer Fiber Surfaces During Electrospinning, Adv. Mater. 19 (2007) 87-91.

[31] X.Y. Sun, L.R. Nobles, H.G. Börner, R.J. Spontak, Field-Driven Surface Segregation of Biofunctional Species on Electrospun PMMA/PEO Microfibers, Macromol. Rapid Commun. 29 (2008) 1455-1460.

[32] R. Gentsch, F. Pippig, S. Schmidt, P. Cernoch, J. Polleux, H.G. Börner, Single-Step Electrospinning to Bioactive Polymer Nanofibers, Macromolecules 44(3) (2011) 453-461.

[33] M.T. Hunley, A. Harber, J.A.Orlicki, A.M. Rawlett, T.E. Long, Effect of Hyperbranched Surface-Migrating Additives on the Electrospinning Behaviour of Poly(Methyl Methacrylate), Langmuir 24 (2008) 654-657.

[34] A. Bianco, G. Iardino, C. Bertarelli, L. Miozzo, A. Papagni, G. Zerbi, Modification of Surface Properties of Electrospun Polyamide Nanofibers by Means of a Perfluorinated Acridine, Appl. Surf. Sci. 253 (2007) 8360-8364.

[35] K. Acatay, E. Simsek, C. Ow-Yang, Y.Z. Menceloglu, Tunable Superhydrophobically Stable Polymeric Surfaces by Electrospinning, Angew. Chem., Int. Ed. 43(39) (2004) 5210-5213.

[36] W.L. Wu, Q.Z. Zhu, F.L. Qing, C.C. Han, Water Repellency on a Fluorine-Contaning Polyurethane Surface: Toward Understanding the Surface Self-Cleaning Effect, Langmuir 25 (2009) 17-20.

[37] W. Wu, G. Yuan, A. He, C.C. Han, Surface Depletion of The Fluorine Content of Electrospun Fibers of Fluorinated Polyurethane, Langmuir 25 (2009) 3178-3183.

[38] Y. Guo, D. Tang, E. Zhao, Z. Yu, H. Lv, X. Li, Controlled Synthesis of Amphiphilic Graft Copolymer for Superhydrophobic Electrospun Fibers with Effective Surface Fluorine Enrichment: The Role of Electric Field and Solvent, RSC Adv., 5 (2015) 82789-82799.

[39] G.R. Choi, J. Park, J.W. Ha, W.D. Kim, H. Lim, Superamphiphobic Web of PTFEMA Fibers via Simple Electrospinning without Functionalization, Macromol. Mater. Eng. 295 (2010) 995-1002.

[40] M. Khayet, R. Wang, Mixed Matrix Polytetrafluoroethylene/Polysulfone Electrospun Nanofibrous Membranes for Water Desalination by Membrane Distillation, ACS Appl. Mater. Interfaces 10 (2018) 24275-24287.

[41] P. Arribas, M. Khayet, M.C. García-Payo, L. Gil, Self-Sustained Electro-Spun Polysulfone Nano-Fibrous Membranes and Their Surface Modification by Interfacial Polymerization for Micro- and Ultra-Filtration, Sep. Purif. Technol. 138 (2014) 118-129.

[42] X. Li, M.C. García-Payo, M. Khayet, M. Wang, X. Wang, Superhydrophobic Polysulfone/Polydimethylsiloxane Electrospun Nanofibrous Membranes for Water Desalination by Direct Contact Membrane Distillation. J. Membr. Sci. 542 (2017) 308−319.

[43] M. Khayet, D.E. Suk, R.M. Narbaitz, J.P. Santerre, T. Matsuura, Study on Surface Modification by Surface-Modifying Macromolecules and its Applications in Membrane-Separation Processes, J. Appl. Polym. Sci. 89 (2003) 2902–2916.

[44] M. Essalhi, M. Khayet, Self-Sustained Webs of Polyvinylidene fluoride Electrospun Nano-fibers: E ects of Polymer Concentration and Desalination by Direct Contact Membrane Distillation, J. Membr. Sci. 454 (2014) 133–143.

[45] M. Essalhi, M. Khayet, Self-Sustained Webs of Polyvinylidene Fluoride Electrospun Nanofibers at Different Electrospinning Times: 1. Desalination by Direct Contact Membrane Distillation, J. Membr. Sci. 433 (2013) 167-179.

[46] M. Khayet, T. Matsuura, Membrane Distillation: Principles and Applications, Elsevier, The Netherlands, 2011.

[47] S.J. Shilton, K.A. Prokhorov, S.A. Gordeyev, G.Y. Nikolaeva, I.R. Dunkin, W.E. Dunkin, W.E. Smith, P.P. Pashinin, Raman Spectroscopic Evaluation of Molecular Orientation in Polysulfone, Laser Phys. Lett. 1 (2004) 336-339.

[48] L.H. Catalani, G. Collins, M. Jaffe, Evidence of Molecular Orientation and Residual Charge in the Electrospinning of Poly(Butylene Terephtalate) Nanofibers, Macromolecules 40 (2007) 1693-1697.

[49] J. Wang, Y. Xu, L. Zhu, J. Li, B. Zhu, Amphiphilic ABA Copolymers Used for Surface Modification of Polysulfone Membranes, Part 1: Molecular Design, Synthesis, and Characterization, Polymer 49 (2008) 3256-3264.

[50] A.B.D. Cassie, S. Baxter, Wettability of Porous Surfaces, Trans. Faraday Soc. 40 (1944) 0546-0550.

[51] M. Khayet, M.C. García-Payo, L. García-Fernández, J. Contreras-Martínez, Dual-Layered Electrospun Nanofibrous Membranes for Membrane Distillation, Desalination 426 (2018) 174-184.

[52] C. Su, J. Chang, K. Tang, F. Gao, Y. Li, H. Cao, Novel Three-Dimensional Superhydrophobic and Strength-Enhanced Electrospun Membranes for Long-Term Membrane Distillation, Sep. Purif. Tech. 178 (2017) 279-287.

[53] Z.Q. Dong, X.H. Ma, Z.L. Xu, Z.Y. Gu, Superhydrophobic Modification of PVDF–SiO_2 Electrospun Nanofiber Membranes for Vacuum Membrane Distillation, RSC Adv. 5 (2015) 67962-67970.

[54] Y. Liao, C.H. Loh, R. Wang, A. G. Fane, Electrospun Superhydrophobic Membranes with Unique Structures for Membrane Distillation. ACS Appl. Mater. Interfaces 6 (2014) 16035-16048.

[55] Y. Liao, R. Wang, A.G. Fane, Fabrication of Bioinspired Composite Nanofiber Membranes with Robust Superhydrophobicity for Direct Contact Membrane Distillation. Environ. Sci. Technol. 48 (2014) 6335-6341.

[56] Y. Liao, R. Wang, A.G. Fane, Engineering Superhydrophobic Surface on Poly(Vinylidene Fluoride) Nanofiber Membranes for Direct Contact Membrane Distillation. J. Membr. Sci. 440 (2013) 77−87.

[57] L.D. Tijing, Y.C. Woo, W.G. Shim, T. He, J.S. Choi, S.H. Kim, H.K. Shon, Superhydrophobic Nanofiber Membrane Containing Carbon Nanotubes for High-Performance Direct Contact Membrane Distillation. J. Membr. Sci. 502 (2016) 158-170.

[58] L.D. Tijing, Y.C. Woo, M.A.H. Johir, J.S. Choi, H.K. Shon, A Novel Dual-Layer Bicomponent Electrospun Nanofibrous Membrane for Desalination by Direct Contact Membrane Distillation. Chem. Eng. J. 256 (2014) 155-159.

[59] B.S. Lalia, I. Janajreh, R.A Hashaikeh, Facile Approach to Fabricate Superhydrophobic Membranes with Low Contact Angle Hysteresis. J. Membr. Sci. 539 (2017) 144-151.

[60] M. Essalhi, M. Khayet, Self-Sustained Webs of Polyvinylidene Fluoride Electrospun Nanofibers at Different Electrospinning Times: 2. Theoretical Analysis, Polarization Effects and Thermal Efficiency, J. Membr. Sci. 433 (2013) 180-191.

[61] X. Li, C. Wang, Y. Yang, X. Wang, M. Zhu, B.S. Hsiao, Dual-Biomimetic Superhydrophobic Electrospun Polystyrene Nanofibrous Membranes for Membrane Distillation, ACS Appl. Mater. Interfaces 6 (2014) 2423-2430.

[62] H. Maab, L. Francis, A. Al-Saadi, C. Aubry, N. Ghaffour, G. Amy, S.P. Nunes, Synthesis and Fabrication of Nanostructured Hydrophobic Polyazole Membranes for Low-Energy Water Recovery, J. Membr. Sci. 423-424 (2012) 11-19.

Membrane code	SEM images and fiber diameter distribution (d_i)			TEM image
PSF-0	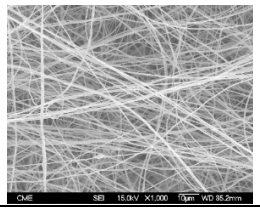	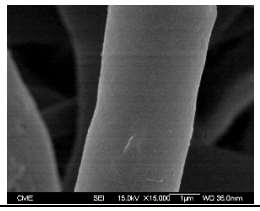	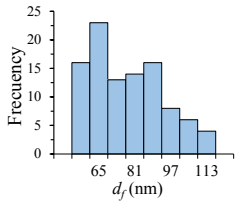	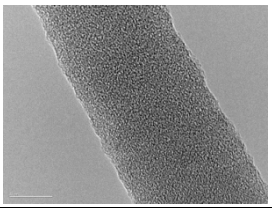
PSF-1.5	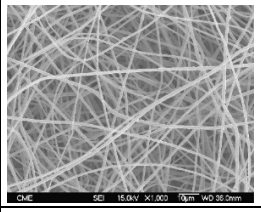	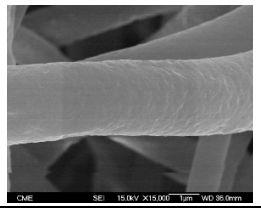	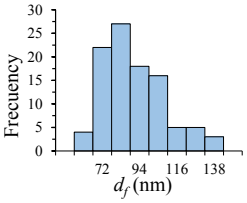	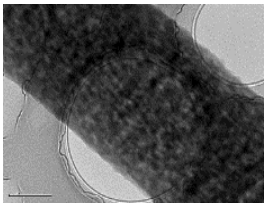
PSF-3	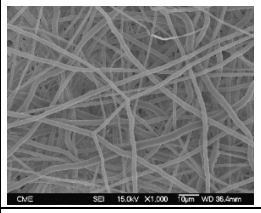	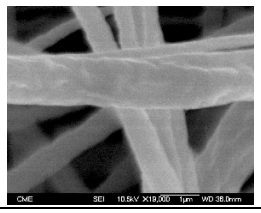	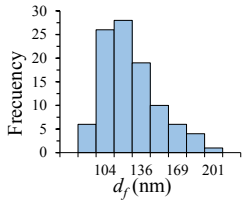	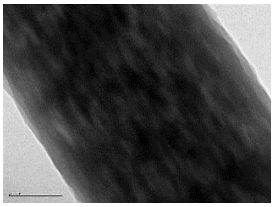
PSF-4.5	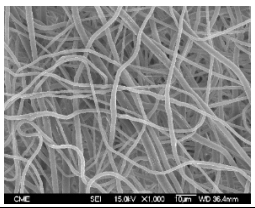	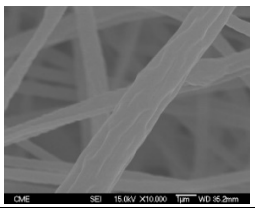	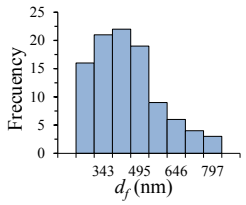	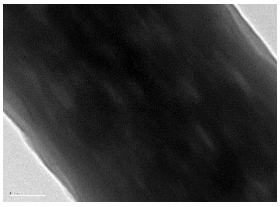
PSF-6	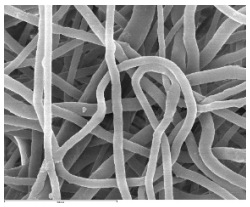	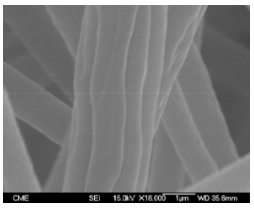	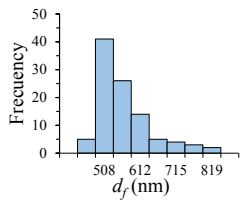	

Figure 1. SEM (left and middle) and TEM (right) images of the PSF and FPA blended PSF ENMs together with their diameter size distribution histograms obtained from SEM images.

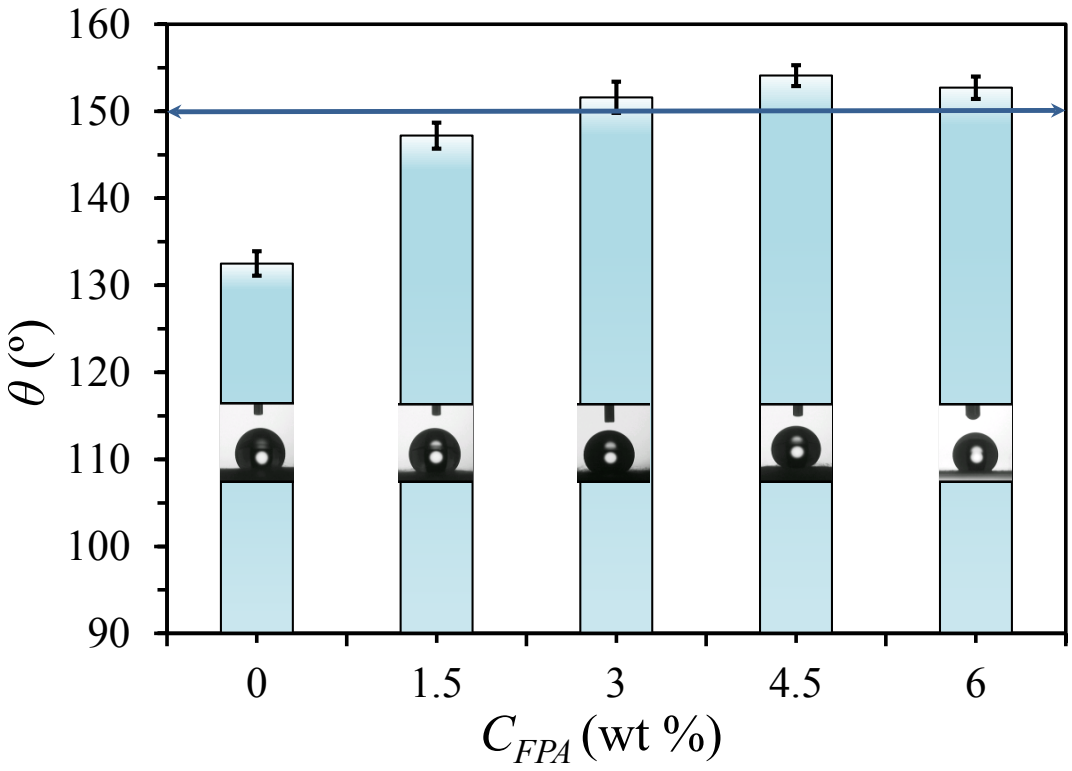

Figure 2. Water contact angle (θ) of the PSF and FPA blended PSF ENMs as a function of FPA concentrations in the electrospinning dope.

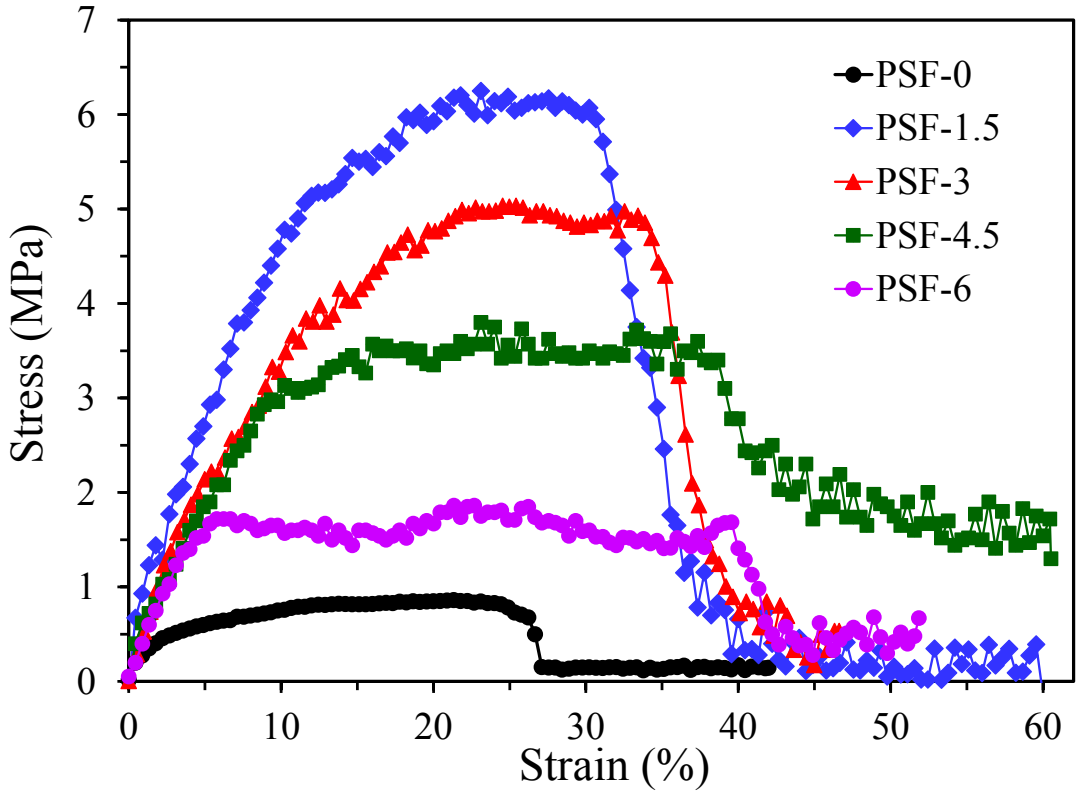

Figure 3. Stress–strain curves of the PSF and FPA blended PSF ENMs for different FPA concentrations.

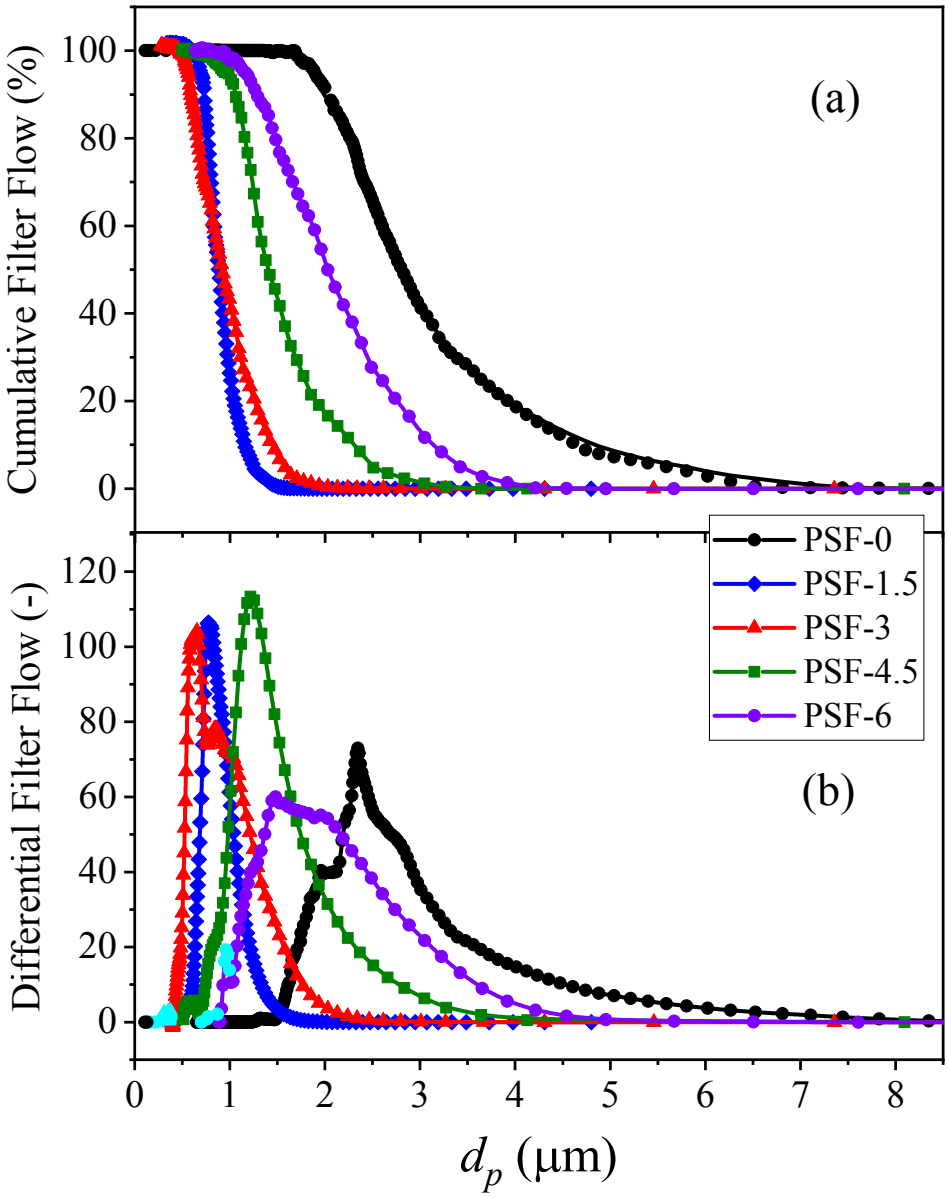

Figure 4. Cumulative (a) and differential (b) filter flow distributions of the inter-fiber space of the PSF and FPA blended PSF ENMs for different FPA concentrations.

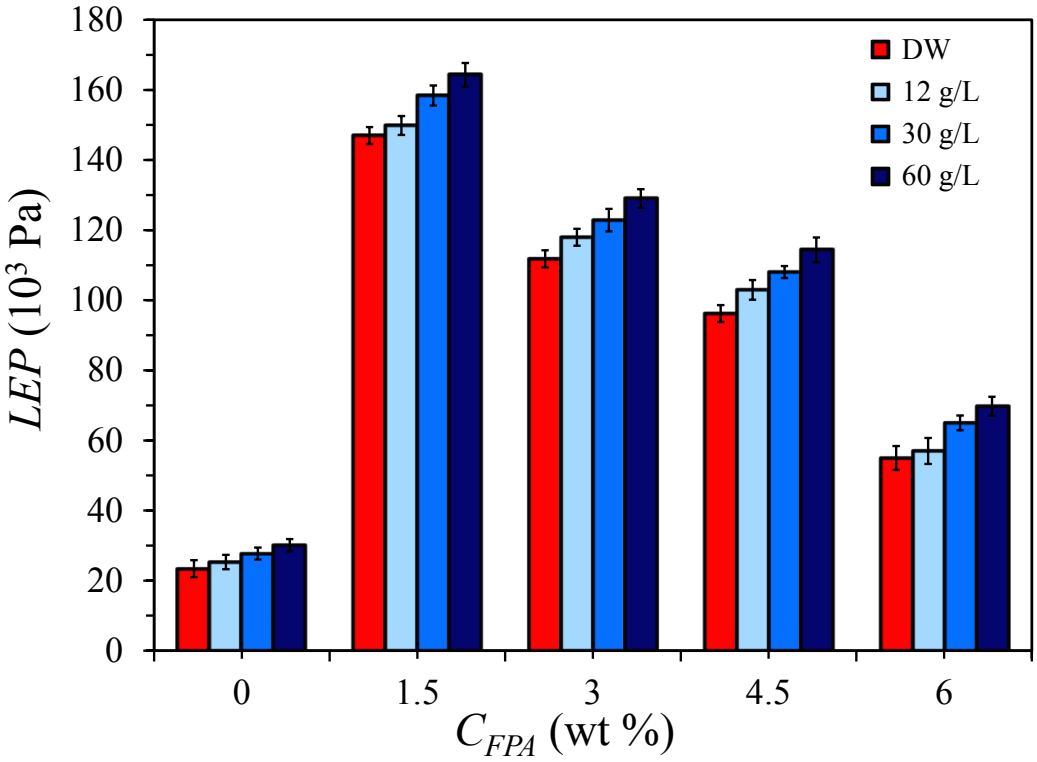

Figure 5. Liquid entry pressure (*LEP*) of distilled water and salt (NaCl) aqueous solutions (12, 30 and 60 g/L) of PSF and FPA blended PSF ENMs for different FPA concentrations in the electrospinning dope.

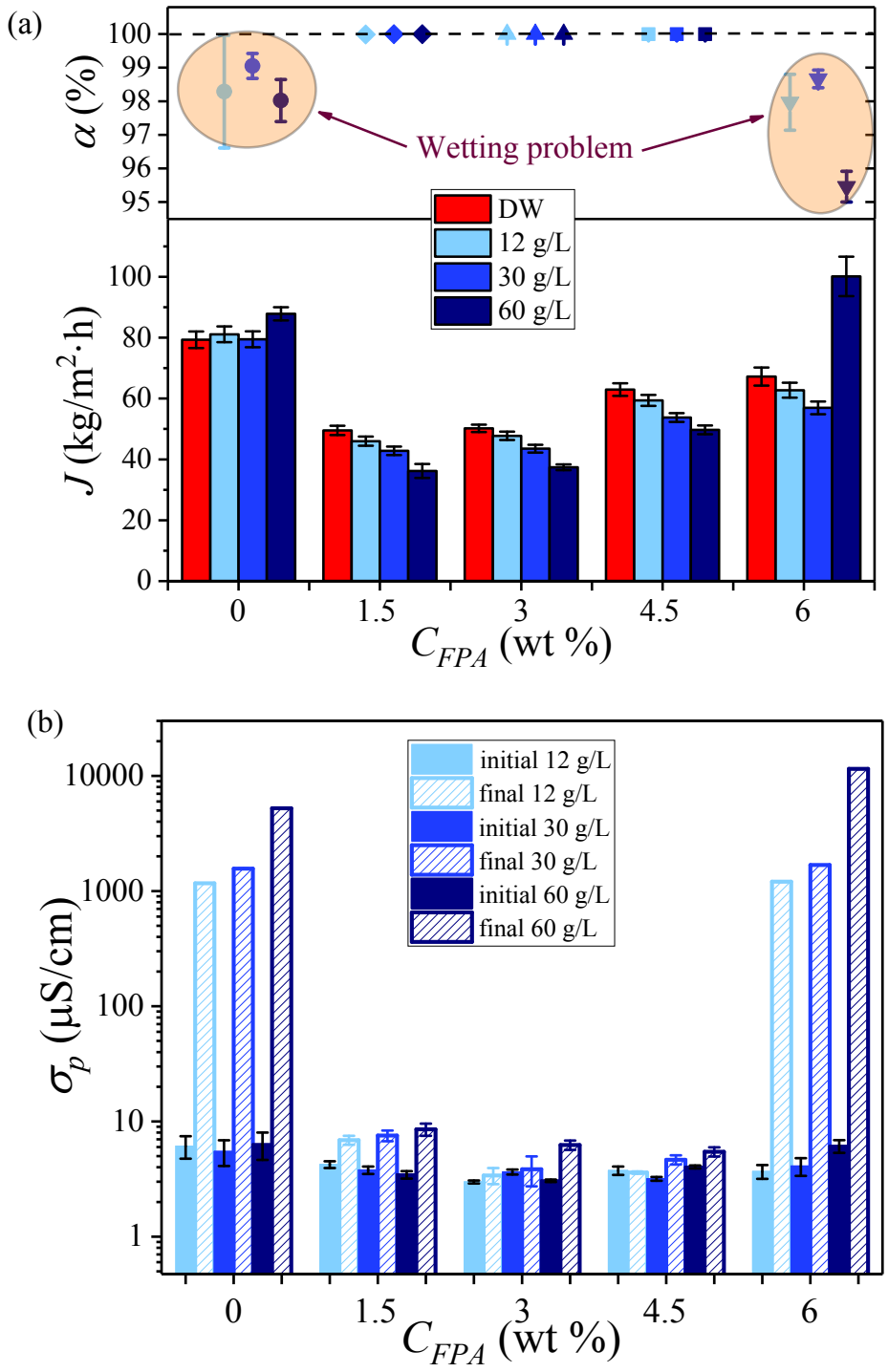

Figure 6. (a) Permeate flux (J) and NaCl rejection factor ($\alpha = (1-C_{b,p}/C_{b,f})\cdot 100$, where $C_{b,f}$ and $C_{b,p}$ are the concentrations of the bulk feed and permeate solutions, respectively), and (b) Initial (I) and final (F) electrical conductivity (σ_p) of the permeate of the PSF and FPA blended PSF ENMs as a function of FPA concentration and for different salt aqueous solutions as feed.

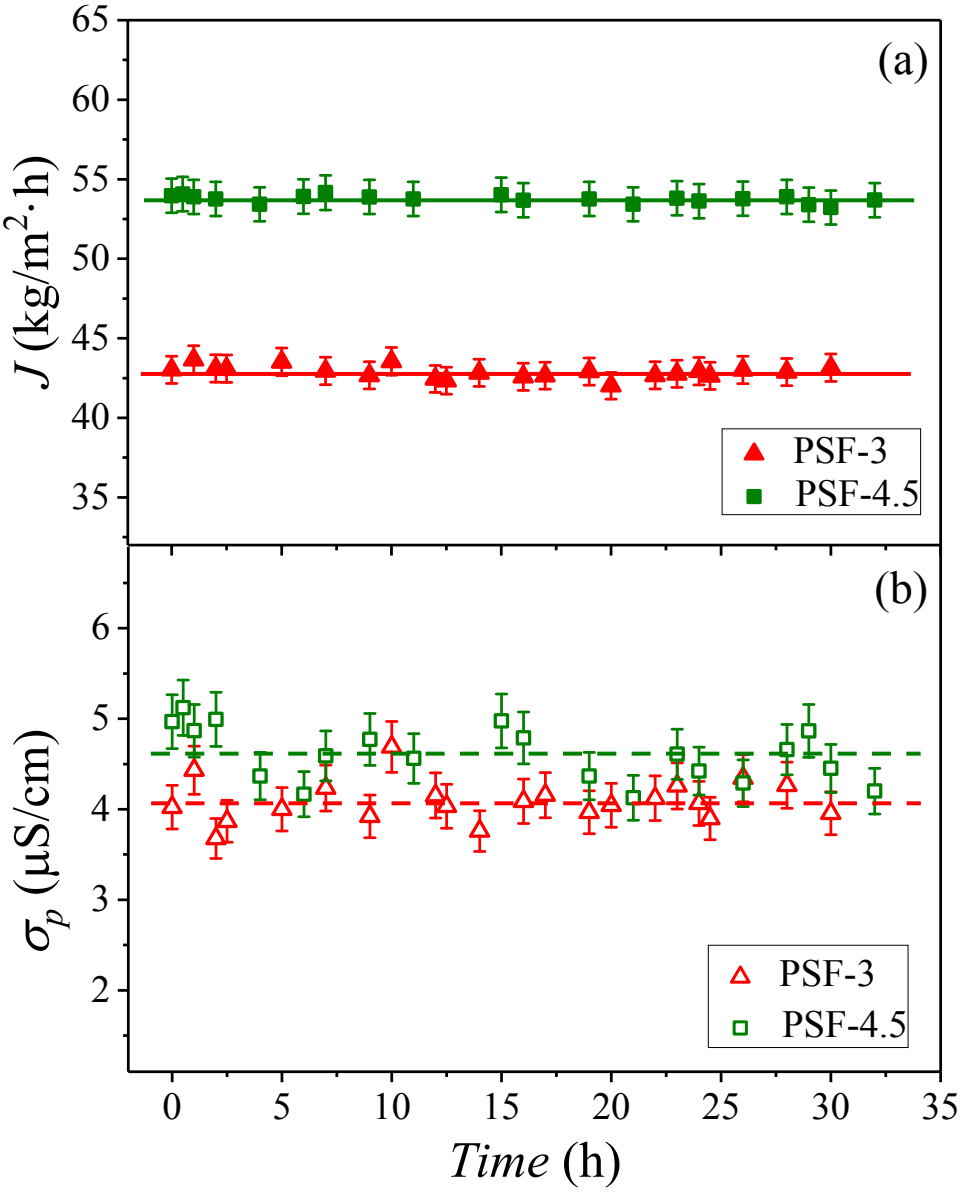

Figure 7. Permeate flux (a) of PSF-3 and PSF-4.5 and their electrical conductivities (b) as a function of DCMD operation time (30 g/L NaCl aqueous solution as feed, T_f = 80ºC, T_p = 20°C, stirring rate 500 rpm).

Tables

Table 1. Surface tension (γ_p), electrical conductivity (σ_p), viscosity (μ_p) of the PSF and FPA blended PSF solutions as well as nanofiber diameter (d_f) of the prepared ENMs.

ENMs	C_{FPA} (wt %)	C_{FPA} (%) [a]	γ_p (mN/m)	σ_p (μS/cm) [b]	μ_p (Pa.s)	d_f (nm)
PSF-0	0	0	41.8 ± 0.5	2.17 ± 0.01	2.00 ± 0.01	78 ± 15
PSF-1.5	1.5	6	27.0 ± 1.8	2.27 ± 0.01	3.28 ± 0.11	91 ± 18
PSF-3	3	12	25.6 ± 0.4	2.57 ± 0.04	4.83 ± 0.05	126 ± 26
PSF-4.5	4.5	18	25.0 ± 0.4	2.72 ± 0.02	6.15 ± 0.05	440 ± 130
PSF-6	6	24	23.3 ± 0.4	2.86 ± 0.01	7.35 ± 0.06	561 ± 80

[a] Amounts based on the PSF polymer weight
[b] σ_p = 0.50 ± 0.01 μS/cm of 80/20 wt % DMAC/acetone mixture

Table 2. Atomic percentage of different elements found on the surface of the PSF and FPA blended PSF ENMs using XPS at different take-off angles.

ENMs	Take-off angle [a] (º)	C-1s (%)	O-1s (%)	F-1s (%)	S-2p (%)	N-1s (%)
PSF-0	15	84.9	11.3	0	3.8	0
	45	86.3	10.7	0	3.0	0
	75	86.7	10.4	0	2.9	0
PSF-1.5	15	62.7	6.6	26.6	1.2	2.9
	45	63.4	6.9	25.6	1.2	3.0
	75	65.6	6.9	22.4	1.5	3.7
PSF-3	15	56.2	6.6	33.5	1.4	2.4
	45	59.0	6.7	30.3	1.2	2.8
	75	66.1	7.5	21.6	1.6	3.2
PSF-4.5	15	52.3	6.5	37.6	1.2	2.3
	45	56.4	6.6	33.4	1.2	2.4
	75	61.6	6.9	27.0	1.3	3.3
PSF-6	15	47.4	5.2	44.0	< 0.1	3.4
	45	51.5	5.8	38.9	< 0.1	3.7
	75	55.5	5.5	35.3	< 0.1	3.7

[a] XPS analysis depth, L_{XPS}, depends on the take-off angle: L_{XPS} (15º) = 2.5 nm; L_{XPS} (45º) = 6.8 nm and L_{XPS} (75º) = 9.3 nm.

Table 3. Mechanical properties (Young's modulus, Y_M; tensile strength, T_S; elongation at break, E_b), thickness (δ), void volume fraction (ε) and mean inter-fiber space (d_i) of the PSF and FPA blended PSF ENMs.

ENMs	Y_M (MPa)	T_S (MPa)	E_b (%)	δ (μm)	ε (%)	d_i (nm)
PSF-0	14.3 ± 1.4	0.85 ±0.03	21.9 ± 0.5	110 ± 9	82.3 ± 0.7	2748 ± 69
PSF-1.5	65.0 ± 0.8	6.0 ± 0.4	31.1 ± 1.6	111 ± 11	84.1 ± 0.2	868 ± 21
PSF-3	52 ± 3	4.4 ± 0.4	34.3 ± 0.8	129 ± 12	87.1 ± 0.8	932 ± 21
PSF-4.5	47 ± 4	3.73 ± 0.24	36.7 ± 1.1	194 ± 21	95.4 ± 0.3	1388 ± 48
PSF-6	32 ± 3	1.48 ± 0.23	39.4 ± 0.3	293 ± 100	97.9 ± 0.2	2011 ± 25

Table 4. Characteristics and MD performance of surface modified superhydrophobic ENMs proposed for desalination.

Material [a]	θ (º)	*LEP* (10^5 Pa)	d_i (µm)	ε (%)	δ (µm)	J (kg/m^2.h)	σ_p (µS/cm) / (α, %)	Ref.
200% FS-SiO_2/PVDF 3 wt % PVDF	154.0	1.5 *	0.32	78.5 *	72	25 (DCMD, 25 h, 60/20ºC, 3.5 g/L NaCl)	< 5 (>99.99%)	[54]
200% FS-SiO_2/PVDF 5 wt % PVDF	150	1.8 *	0.36	65 *	76	21 (DCMD, 40 h, 60/20ºC, 3.5 g/L NaCl)	< 5 (>99.99%)	[54]
200% FS-SiO_2/PVDF 5 wt % PVDF	156 ± 2	1.79 ± 0.07	0.77 ± 0.02	83 ± 1	129 ± 8	18.9 (DCMD, 50 h, 60/20ºC, 3.5 g/L NaCl)	< 5	[55]
Ag/PDA/PVDF [b]	153 ± 4	1.46 ± 0.12	0.34 ± 0.01	77 ± 1	47 ± 4	31.6 (DCMD, 8 h, 60/20ºC, 35 g/L NaCl)	< 5	[56]
5% CNT/PVDF-HFP	158.5	0.99	0.29	84 ± 1	81	29.5 (DCMD, 5 h, 60/20ºC, 35 g/L NaCl)	< 1 (99.99%)	[57]
PVDF-HPF/PAN (25/75)	150	0.94	1	90	82	30 (DCMD, 3 h, 60/20ºC, 35 g/L NaCl)	(> 98.5%)	[58]
334 % M-SiO_2/PVDF	152 ± 1	1.64 ± 0.11	0.23	79	173 ± 8	25 (DCMD, 100 h, 60/15ºC, 35 g/L NaCl)	< 5	[52]
2 wt % FAS grafted PVA (10 wt % PVA)	158 ± 2	1.79 ± 0.03	0.46 ± 0.01	82 ± 2	100 ± 3	25.2 (VMD, 16 h, 60ºC, 9 kPa, 35 g/L)	< 5	[9]
PPFDA/ PA6(3)T [c]	151 ± 2	3.73	-	69	55 ± 2	11 (AGMD, 3 h, 70/25ºC, 35 g/L)	(99.99%)	[13]
OTFE/PVDF-HFP	156 ± 2	2.4 – 2.8	0.18 – 0.22	60	125 ± 25	13-14 (DCMD, 3 h, 67/25ºC, 20 g/L)	130 (99.9%)	[59]
PDMS/PSF (1 g in hexane, 23 wt % PSF)	151.1 ± 1.1	0.7	2.819	82	97 ± 5	21.5 (DCMD, 12 h, 70/20ºC, 30 g/L)	4.224 - 4.523	[42]
PSF-3	151.6 ± 1.8	1.23 ± 0.03 [d]	0.932 ± 0.021	87.1 ± 0.8	129 ± 12	42.88 ± 0.39 (DCMD, 30 h, 80/20ºC, 30 g/L) 29.89 ± 0.15 (DCMD, 3 h, 65/20ºC, 30 g/L)	4.1 ± 0.2 3.9 – 4.3	This study
PSF-4.5	154.1 ±1.2	1.08 ±0.02 [d]	1.388 ±	95.4 ± 0.3	194 ± 21	53.76 ± 0.24 (DCMD, 32	4.6 ± 0.3	This

	0.048	h, 80/20ºC, 30 g/L) 33.47 ± 0.18 (DCMD, 3 h, 65/20ºC, 30 g/L)	4.5 – 4.7	study

* Values estimated from the given figure

[a] For filled ENMs, the concentration of filler is based on the polymer weight

[b] Multi-step modification procedure

[c] PA6(3)T ENM coated by PPFDA using initiated chemical vapor deposition (iCVD)

[d] For 30 g/L NaCl solution

Abbreviations: PVDF (polyvinylidene fluoride), PVDF-HFP (polyvinylidene fluoride-hexafluoropropylene), PAN (polyacrylonitrile), PVA (poly(vinyl alcohol)), PDMS (polydimethylsiloxane), PSF (polysulfone), PDA (poly-dopamine), FAS (fluoroalkylsilane), PPFDA (poly(1H,1H,2H,2H-perfluorodecyl acrylate)), PA6(3)T (poly(trimethyl hexamethylene terephthalamide)), OTFE (tetrafluoroethylene oligomers), FS-SiO_2 (modified silica by α,ω-triethoxysilane-terminated perfluoropolyether ($(EtO)_3Si$-PFPE$Si(OEt)_3$), M-SiO_2 (modified SiO_2 by octamethylcyclotetrasiloxane, AEROSIL R106), Ag (silver nanoparticle), CNT (carbon nanotube), DCMD (direct contact membrane distillation), VMD (vacuum membrane distillation), AGMD (air gap membrane distillation).

Supporting Information

Superhydrophobic Nanofibers Electrospun by Surface Segregating Fluorinated Amphiphilic Additive for Membrane Distillation

M. Khayet[1,2,*], C. García-Payo[1], T. Matsuura[3]

[1] Department of Structure of Matter, Thermal Physics and Electronics, Faculty of Physics, University Complutense of Madrid, Avda. Complutense s/n 28040 Madrid (Spain)

[2] Madrid Institute of Advances Studies of Water (IMDEA Water Institute), Calle Punto Com n° 2, 28805 Alcalá de Henares, Madrid (Spain)

[3] Department of Chemical and Biological Engineering, University of Ottawa, 161 Louis Pasteur St., Ottawa, ON, K1N 6N5 (Canada)

* Corresponding authors: khayetm@ucm.es (M. Khayet)

1. Synthesis and chemical structure of fluorinated polyurethane additive (FPA).

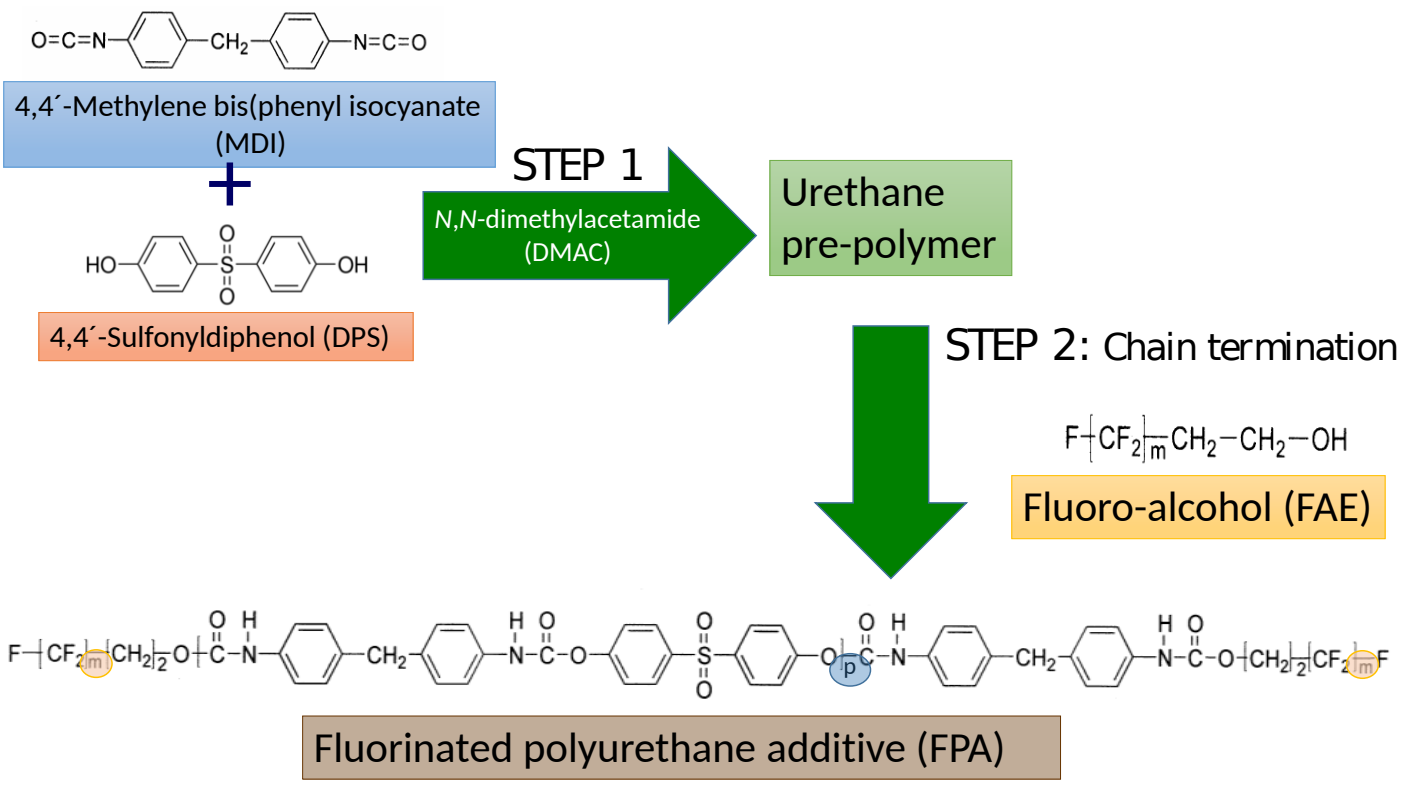

m [a]	p [b]	F (wt %)	M_w (10^4) [c]	M_n (10^4) [c]	M_w/M_n
7.58	4.42	20.0 ± 0.1	0.6 ± 0.1	0.5 ± 0.1	1.2

[a] Determined from the molecular weight of FAE.

[b] Determined from the fluorine content of FPA.

[c] M_w and M_n values are reported as polystyrene equivalent average molecular weights.

Figure S1. *Synthesis, chemical structure and characteristics of the used fluorinated polyurethane additive (FPA).*

2. X-ray photoelectron spectroscopy (XPS) diagrams of FPA/PSF blended ENMs shown as examples

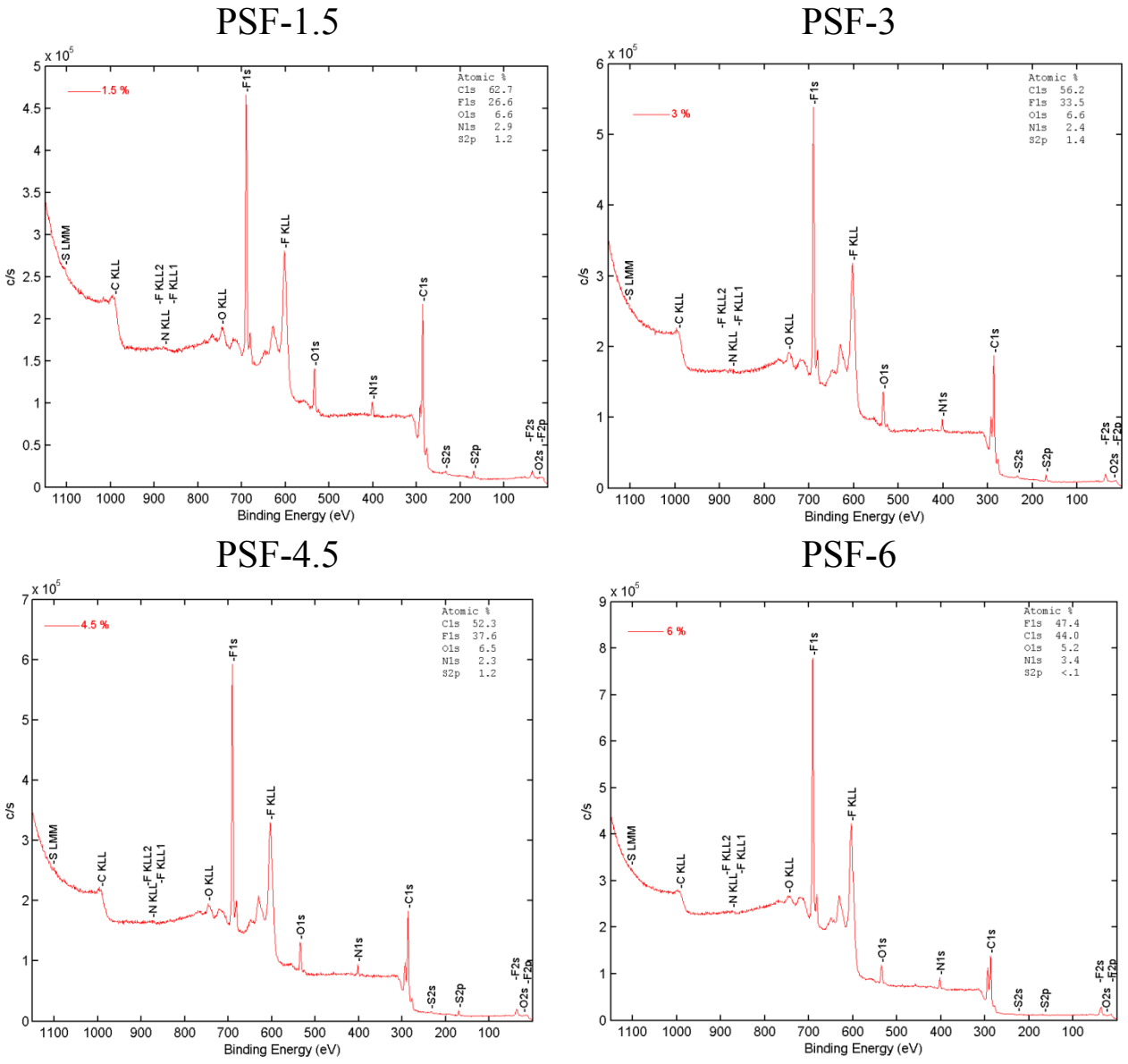

Figure S2. *Typical XPS diagrams of FPA/PSF blended ENMs at a take-off angle of 15°, which corresponds to 2.5 nm from the top surface of the samples.*

The XPS diagrams show the characteristic peaks of oxygen (O-1s) and sulphur (S-2p) atoms of both PSF and FPA detected at 531 and 167.8 eV, respectively; and the peaks of the binding energy

at 685.7 eV and 400.2 eV of fluorine (F-1s) and nitrogen (N-1s) atoms associated to FPA. From the peak intensity of each element, the atomic percentage was evaluated using PHI ACCESS ESCA-V6.0F software package.

3. *Table S1.* *Theoretical atomic composition of PSF and FPA blended PSF ENMs.*

ENMs	C (%)	O (%)	F (%)	S (%)	N (%)	H (%)
PSF-0	73.31	14.47	0	7.25	0	4.97
PSF-1.5	72.22	14.47	1.10	7.07	0.27	4.87
PSF-3	71.12	14.48	2.20	6.89	0.54	4.77
PSF-4.5	70.03	14.49	3.30	6.71	0.82	4.66
PSF-6	68.93	14.50	4.40	6.53	1.09	4.56

The calculation was based on the molecular structure of FPA assuming uniform distribution of FPA in the blended ENMs shown in Table S2.

Table S2. *Atomic composition of FPA.*

Additive	C (%)	O (%)	F (%)	S (%)	N (%)	H (%)
FPA	55.07	14.58	18.34	4.23	4.54	3.24

The host polymer PSF has the four elements C, O, S and H while the additive FPA has the additional elements F and N. With the addition of FPA the amount of C was reduced whereas that of O was maintained the same because FPA also has O. The content of F and N in the FPA blended PSF ENMs increased gradually with the increase of the FPA amount in the blends. On the contrary,

the amounts of S and H were decreased. The XPS elemental analysis summarized in Table 2 provided different results due to the fact that the theoretical calculations were based on uniform distribution of FPA in the FPA blended PSF ENMs.

4. Water contact angle of the PSF and FPA blended PSF ENMs as a function of the electrospun fiber size.

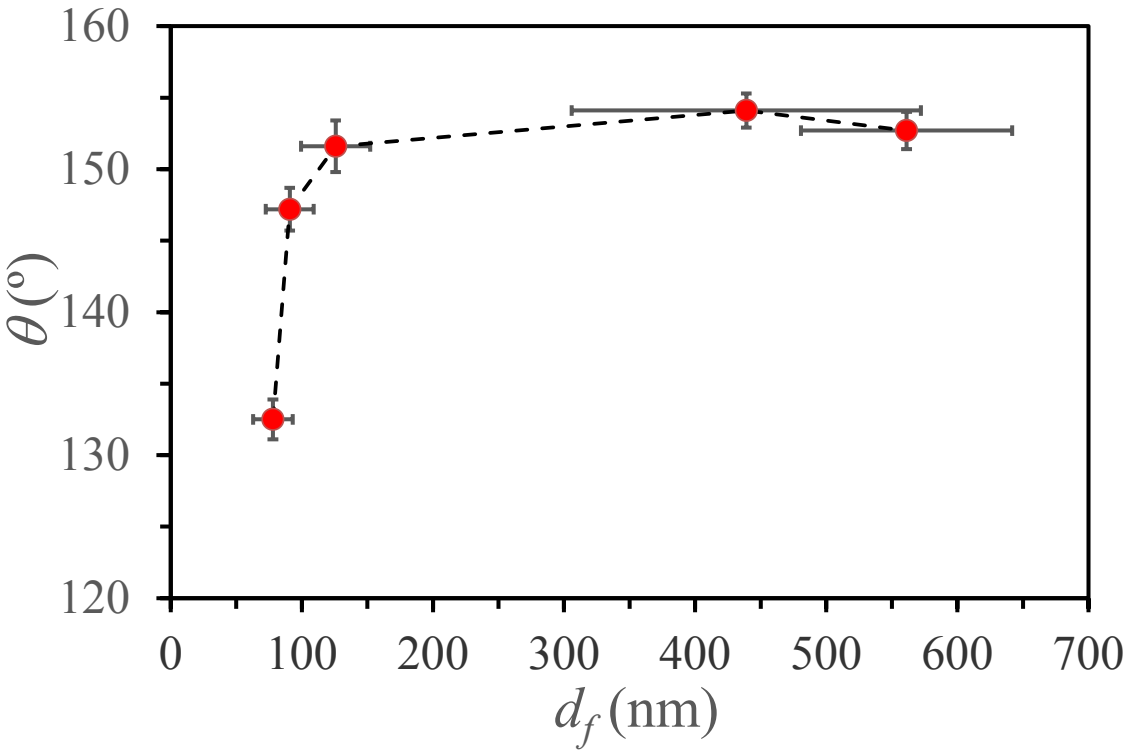

Figure S3. *Water contact angle (θ) vs. fiber diameter (d_f) of the PSF and FPA blended PSF ENMs.*

Following Cassie and Baxter model,[58] smaller nanofibers diameters result in larger fraction of air pockets generated on ENMs and higher apparent contact angles. An opposite trend was observed in Figure S3 between the water contact angle (θ) and the fiber diameter (d_f). This also indicated that other physico-chemical characteristics of the electrospun nanofiber surface affected the

contact angle of ENMs (i.e. the increase of the fluorine amount and the corrugated structure of the nanofiber surface with the increase of FPA in the PSF electrospinning solution).

5. Mechanical properties of FPA blended PSF ENMs as a function of FPA amount in the PSF electrospinning solution.

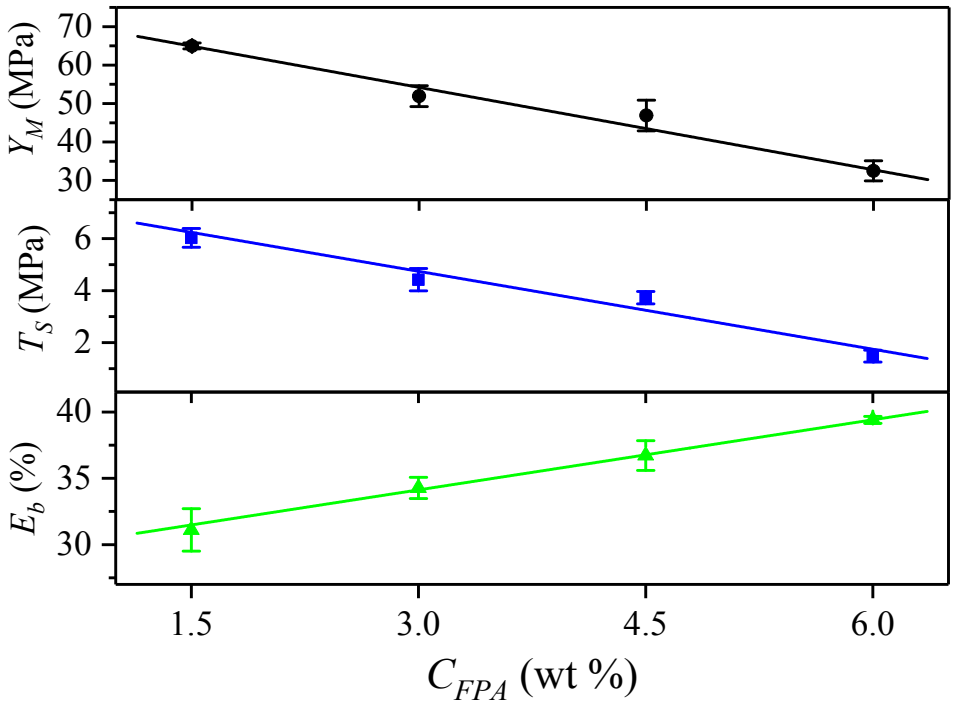

Figure S4. *Y_M , T_S and E_b as a function of the FPA amount in the PSF electrospinning solution*

Figure S4 shows a gradual decrease of Y_M and T_S against FPA content in the PSF host polymer blend with reasonably high correlation coefficients, 0.9872 and 0.9617, respectively. However, E_b was gradually increased with the increase of the FPA amount in the PSF blend solution being the correlation coefficient of the linear plot 0.9978.

6. Inter-fiber space of the PSF and FPA blended PSF ENMs.

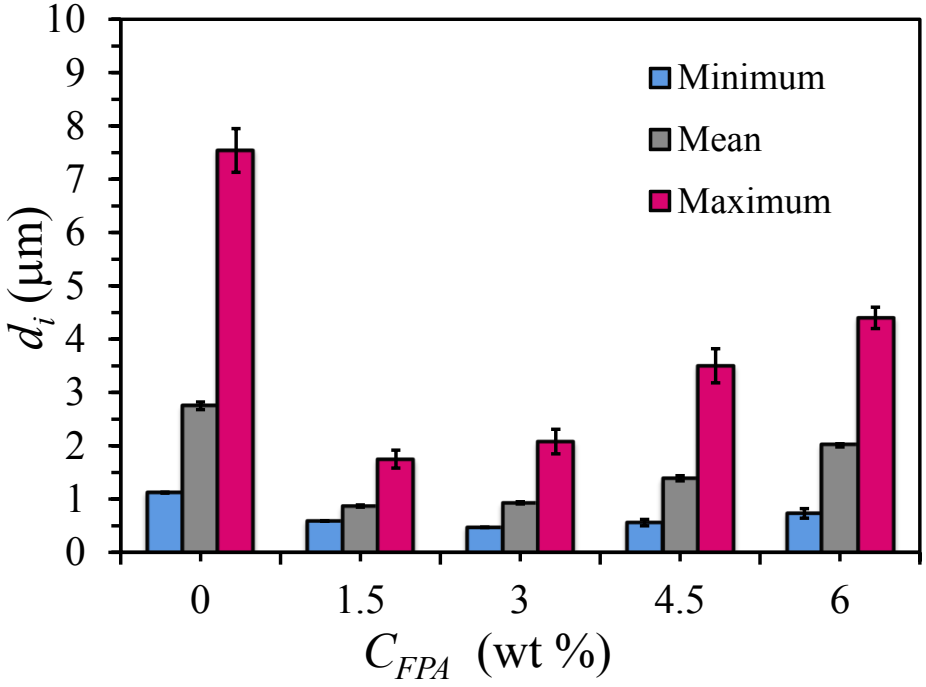

Figure S5. *Maximum, mean and minimum size of the inter-fiber space (d_i) of the PSF and FPA blended PSF ENMs.*

Figure S5 shows the minimum, mean and maximum size of the inter-fiber space of PSF and FPA blended PSF ENMs prepared with different amounts of FPA in the electrospinning dope. The FPA blended PSF ENMs exhibited smaller d_i values than the PSF ENM (PSF-0). Upon addition of FPA to PSF host polymer solution, it can be seen the significant reduction of the maximum size of the inter-fiber space compared to the decrease of the mean and minimum sizes of the inter-fiber space (PSF-0 and PSF-1.5). An enhancement of d_i (minimum, mean and maximum) with the increase of FPA content in the electrospinning dope was observed.